RESEARCH ARTICLE

The FASEB Journal

Inhibition of triglyceride metabolism-associated enhancers alters lipid deposition during adipocyte differentiation

Sha Zeng[1,2] | Ziqi Li[1,2] | Xiaokai Li[3,4] | Qinjiao Du[1,2] | Yu Zhang[1,2] | Zhining Zhong[1,2] | Haoming Wang[1,2] | Songling Zhang[1,2] | Penghao Li[5] | Haohuan Li[6] | Li Chen[3,4] | Anan Jiang[1,2] | Peng Shang[7] | Mingzhou Li[1,2] | Keren Long[1,2,3,4]

[1]State Key Laboratory of Swine and Poultry Breeding Industry, Sichuan Agricultural University, Chengdu, China

[2]College of Animal Science and Technology, Sichuan Agricultural University, Chengdu, China

[3]Chongqing Academy of Animal Sciences, Chongqing, China

[4]National Center of Technology Innovation for Pigs, Chongqing, China

[5]Jinxin Research Institute for Reproductive Medicine and Genetics, Sichuan Jinxin Xi'nan Women's and Children's Hospital, Chengdu, China

[6]College of Veterinary Medicine, Sichuan Agricultural University, Chengdu, China

[7]Animal Science College, Tibet Agriculture and Animal Husbandry University, Linzhi, China

Correspondence
Mingzhou Li and Keren Long, State Key Laboratory of Swine and Poultry Breeding Industry, Sichuan Agricultural University, Chengdu 611130, China.
Email: mingzhou.li@sicau.edu.cn and keren.long@sicau.edu.cn

Abstract

Triglyceride (TG) metabolism is a complex and highly coordinated biological process regulated by a series of genes, and its dysregulation can lead to the occurrence of disorders in lipid metabolism. However, the transcriptional regulatory mechanisms of crucial genes in TG metabolism mediated by enhancer–promoter interactions remain elusive. Here, we identified candidate enhancers regulating the *Agpat2*, *Dgat1*, *Dgat2*, *Pnpla2*, and *Lipe* genes in 3T3-L1 adipocytes by integrating epigenomic data (H3K27ac, H3K4me1, and DHS-seq) with chromatin three-dimensional interaction data. Luciferase reporter assays revealed that 11 enhancers exhibited fluorescence activity. The repression of enhancers using the dCas9-KRAB system revealed the functional roles of enhancers of *Dgat2* and *Pnpla2* in regulating their expression and TG metabolism. Furthermore, transcriptome analyses revealed that inhibition of Dgat2-En4 downregulated pathways associated with lipid metabolism, lipid biosynthesis, and adipocyte differentiation. Additionally, overexpression and motif mutation experiments of transcription factor found that two TFs, PPARG and RXRA, regulate the activity of Agpat2-En1, Dgat2-En4, and Pnpla2-En5. Our study identified functional enhancers regulating TG metabolism and elucidated potential regulatory

Sha Zeng, Ziqi Li and Xiaokai Li contributed equally to this work.

- -

mechanisms of TG deposition from enhancer–promoter interactions, providing insights into understanding lipid deposition.

KEYWORDS

adipogenesis, enhancer, key genes, transcriptional regulation, triglyceride

1 | INTRODUCTION

Adipose tissue, serving as the body's energy reservoir, regulates complex processes such as reproduction,[1] inflammation,[2] and immune responses,[3] maintaining energy balance through triglyceride metabolism.[4] Dysfunctions in enzymes associated with triglyceride (TG) synthesis and breakdown disrupt lipid metabolism and disturb energy equilibrium, leading to conditions such as hyperlipidemia, insulin resistance, fatty liver, and glucose metabolism disorders.[5,6] These disruptions increase the risk of metabolic syndrome, including cardiovascular diseases and type 2 diabetes.[7] TG synthesis and breakdown play critical roles in adipose tissue development, with enzymes coordinating to regulate TG balance within adipose tissue.

The synthesis and breakdown of TGs are regulated by a series of genes that encode enzymes involved in lipid metabolism. *Agpat2* is a key critical gene for TG synthesis, encoding 1-acylglycerol-3-phosphate O-acyltransferase 2 (AGPAT2). This enzyme catalyzes the binding of fatty acids to glycerol-3-phosphate, thus forming TG. Notably, *Agpat2* deficiency impairs TG synthesis and storage and leads to the failure of adipocyte differentiation.[8] Moreover, *Agpat2* mutations can lead to congenital generalized lipodystrophy, an autosomal recessive genetic disorder, that is characterized by a lack of adipose tissue in childhood, severe insulin resistance, hypertriglyceridemia, and hepatic steatosis.[9,10] Diacylglycerol O-acyltransferase (DGAT) 1 and 2 are two rate-limiting enzymes that are responsible for catalyzing the final step of TG synthesis.[11–14] Mice lacking *Dgat1* are viable but have reduced TG stores, whereas *Dgat2* knockout mice die soon after birth and have >90% reduction of TGs, indicating that DGAT2 is more important than DGAT1 for TG storage.[13,15–18] In healthy male subjects, oral administration of the DGAT1 inhibitor AZD7687 attenuates postprandial TG excursion, although an increased dose of AZD7687 results in nausea, vomiting, and diarrhea.[19] In addition, the synthesis of TG by DGAT1 protects adipocytes from lipid-induced endoplasmic reticulum stress during lipolysis.[20] Together, these findings indicate that DGAT1 and DGAT2 have overlapping and different functions in adipocytes. Both

Pnpla2[21,22] and *Lipe*[23–26] are crucial genes in the metabolism and breakdown of TGs. *Pnpla2* encodes the enzyme adipose TG lipase (ATGL), which catalyzes the first step of TG hydrolysis.[27] Mutations in *Pnpla2* lead to the onset of neutral lipid storage disease with myopathy or TG deposit cardiomyovasculopathy.[28] By contrast, *Lipe* encodes hormone-sensitive lipase (HSL),[29–31] and its mutation or knockout can affect TG breakdown, potentially leading to issues such as fat accumulation, obesity, and fatty liver disease.[32–35] Although the functions of these genes in TG metabolism have been extensively investigated, research into the regulation of their transcriptional expression remains relatively limited.

Enhancers are critical *cis*-regulatory elements that are distributed throughout the mammalian genome; they serve as spatial and temporal switches in the regulation of gene expression.[36,37] In mammalian cells, active enhancers are enriched in histone 3 lysine 27 acetylation (H3K27ac) and histone 3 lysine 4 monomethylation (H3K4me1).[38–41] Several studies have highlighted the specific roles of histone modifications H3K27ac and H3K4me1 in the identification of candidate enhancers.[42,43] H3K27ac is a marker of active regulatory elements, distinguishing active enhancers and promoters from their inactive counterparts.[41] H3K4me1 is associated with regulatory elements linked to enhancers and other distal elements, but it is also enriched downstream of transcription start sites.[42] In contrast, H3K4me3 is primarily a marker for promoters and transcription-associated regulatory elements.[44] Active enhancer regions are typically found in an open chromatin state,[45] which can be detected using an assay for DNase I hypersensitive sites sequencing (DHS-seq)[46] and the assay for transposase-accessible chromatin with high-throughput sequencing (ATAC-seq).[47,48] Active enhancers can activate gene transcription by recruiting transcription factors (TFs),[49,50] RNA polymerase II,[51] p300,[52] mediator complex,[53] and other factors.[54,55] Research indicates that enhancers can modulate gene expression through chromatin interactions, thereby influencing lipid metabolism.[56–59] Armor et al.[58] identified a liver-specific enhancer that regulates the expression of the lipolysis inhibitor G0/G1 switch gene 2 (G0S2) and plays a crucial role in maintaining lipid homeostasis through

the transcriptional activation of HNF4α. Liru Zhang et al.[59] discovered that MAE-enhancers regulate lipid metabolism-related genes (*ACAT1*, *OXSM*, and *VAPA*). Notably, although enhancers play a key role in regulating gene expression, there is as yet relatively limited research into enhancers that regulate genes associated with TG metabolism.

In the present study, we identified enhancers for *Agpat2*, *Dgat1*, *Dgat2*, *Pnpla2*, and *Lipe* in 3T3-L1 adipocytes. We then evaluated the activity of these enhancers and investigated their roles in the transcription regulation of target gene expression and adipocyte differentiation. Transcriptomic analysis indicates that inhibition of enhancer activity affects adipogenesis pathways. Additionally, we have demonstrated that Retinoid X Receptor α (RXRA) and Peroxisome Proliferator-Activated Receptor γ (PPARG) are involved in the activity of three functional enhancers. These findings provide insights into the molecular determinants of the transcriptional expression of lipid metabolism-related genes and contribute to an enhanced understanding of the roles of enhancers in lipid deposition.

2 | MATERIALS AND METHODS

2.1 | Cell culture and adipocyte differentiation

The 3T3-L1 (Mouse embryo preadipocyte)[60] and H293T (Human embryonic kidney) cell lines were acquired from the Cell Bank of the Chinese Academy of Sciences (Shanghai, China). Both 3T3-L1 and H293T cells were cultivated in Dulbecco's modified Eagle medium (DMEM) high glucose supplemented with 10% fetal bovine serum (Gibco, USA) and 1% penicillin–streptomycin (Invitrogen, USA) at a temperature of 37°C in 5% CO_2 environment. To induce adipocyte differentiation in 3T3-L1 cells, a standard adipogenic MDI cocktail (MDI: IBMX, dexamethasone, and insulin) was employed.[61] In brief, 3T3-L1 cells were seeded in 12-well plates or T25 flasks. Subsequently, cells were allowed to grow until reaching 100% confluence, defined as −2 day (D-2) of 3T3-L1 cell differentiation induction. Upon achieving confluence, cells were further cultured for 48 h, designated as 0 day (D0). After 48 h, the MDI mixture (2 μg/mL dexamethasone, 0.5 mM IBMX, and 10 μg/mL insulin) in DMEM with 10% FBS was added to the cells and incubated for 48 h. Subsequently, cells were cultured in DMEM containing 10 μg/mL insulin and 10% FBS, with medium renewal every 2 days until lipid droplets were observed, typically on the 7th-day post-differentiation induction.

2.2 | Oil Red O staining and BODIPY 493/503 staining

To observe the differentiating adipocytes, cells were seeded in 12-well plates and cultured. The differentiating adipocytes were observed by phase contrast imaging using a Leica DMI6000 B inverted microscope. For the detection of lipid droplets, Oil Red O and BODIPY 493/503 staining was performed. For Oil Red O staining (OriCell®, USA), cells were washed twice with PBS and fixed with 4% paraformaldehyde. Subsequently, prepare an Oil Red O working solution by mixing distilled water and Oil Red O in a ratio of 2:3. After thorough mixing, centrifuge at 250 × g for 4 min. Use the supernatant for staining. After removing the Oil Red O solution, the cells were washed twice with PBS, and the lipid droplets were visualized using a Leica DMI6000 B inverted microscope.

For BODIPY 493/503 staining, the cells were fixed by incubating them with 4% paraformaldehyde for 10 min. After fixation, the cells were washed three times with PBS and then for lipid droplet staining, the fixed cells were exposed to 5 μM BODIPY 493/503 (Invitrogen, USA) in the dark for 20 min. Following another three washes with PBS, to stain the nuclei, the cells were treated with DAPI staining solution (Beyotime, China) for 3 min at RT. Following three washes with PBS, the cells were visualized using a Zeiss Axio Observer 7 inverted fluorescent microscope.

2.3 | RNA isolation, cDNA synthesis, and quantitative real-time PCR (qRT-PCR)

The total RNA was extracted using TRIzol reagent (Invitrogen, USA) following the manufacturer's instructions. Subsequently, the extracted RNA (1 μg) was reverse-transcribed into cDNA using the HiScript III RT SuperMix (Vazyme, China). The diluted cDNA served as the template for RT-PCR amplification. The RT-PCR amplification was conducted on the CFX Connect™ Real-Time System (Bio-Rad, USA) utilizing the ChamQ Universal SYBR qPCR Master Mix (Vazyme, China). The amplification protocol included an initial step at 95°C for 5 min, followed by 40 cycles at 95°C for 10 s and 60°C for 30 s. After the PCR amplification, a melting curve analysis was performed by heating the samples to 95°C for 15 s, cooling to 60°C for 1 min, and then raising the temperature to 95°C for 15 s to confirm primer specificity. The fold difference in gene expression was normalized to the housekeeping gene *β-actin*. All experiments were conducted in triplicate or more for reliable results. The primer sequences for qRT-PCR can be found in Table S1.

2.4 | ChIP-seq and DHS-seq data processing and analysis

We retrieved publicly available ChIP-seq and DHS-seq data from the EBI ENA database (https://www.ebi.ac.uk/ena/browser/home). To align the datasets to the mouse reference genome (mm10), we employed bowtie2 (v2.4.2) with default parameters. To ensure reliable data analysis, PCR duplicates were eliminated using either Samtools (v1.11) or Picard tools (v1.124). MACS2 (v2.2.7.1) was utilized for peak calling, employing a *q*-value cutoff of .05 as the threshold. For generating figures, we converted the data to bigwig files using the bedGraphToBigWig tool (v4), which was subsequently used as input for the tracks. Visualization was performed using the IGV software (v2.10.0), utilizing the generated bigwig files. Table S2 contains comprehensive information regarding these datasets.

2.5 | Identification of gene activity enhancers

We established stringent criteria for identifying the active enhancers of genes. Firstly, we integrated active chromatin status data, including chromatin immunoprecipitation sequencing (ChIP-seq) for H3K27ac and H3K4me1, along with DHS-seq data. We selected regions simultaneously enriched for peaks in these datasets as candidate enhancer regions. Secondly, enhancers often contact with the promoters of targeted genes via long-range chromatin interaction.[62,63] Chromatin interaction data were employed to delineate the interacting relationship between enhancers and target genes. Lastly, regions characterized by the chromatin features of active enhancers and displaying chromatin interactions with promoters are identified as active enhancers of the gene. Detailed information about the identified enhancers is provided in Table S3.

2.6 | Construction of vectors and luciferase reporter assays

We amplified putative active enhancers from the genomic DNA of 3T3-L1 cells and inserted them upstream of the luciferase gene in the pGL3 promoter vector (Promega, USA) at the KpnI site. The integrity of the constructs was confirmed through Sanger sequencing. 3T3-L1 adipocytes were transfected with 95 ng of the respective construct and 5 ng of the Renilla vector using Lipofectamine 3000 (Thermo Fisher Scientific, USA). After 36 h post-transfection, luciferase activity was measured on a GloMax 96-well plate luminometer (Promega, USA) using the Dual-Glo Luciferase Assay kit (Promega, USA) as per the manufacturer's instructions. Firefly luciferase activity was normalized to Renilla luciferase activity and calculated relative to the empty pGL3 promoter vector as a reference. The experiment was conducted in triplicate, with at least one repetition. Results are presented as the mean and its corresponding standard deviation (mean ± SD). PCR primer sequences used for constructing the vectors can be found in Table S3.

2.7 | Evolutionary conservation analysis of active enhancers

The conservation of active enhancers was evaluated using the phastCons method within the UCSC genome browser (http://genome-asia.ucsc.edu/). To assess conservation, placental mammals were analyzed. Each enhancer element was assigned a log-odds score (LOD), which represents the logarithm of its probability under the conserved model minus its probability under the nonconserved model. The "score" field provides transformed values ranging from 0 to 1000, while the raw log-odds scores are retained in the "name" field. The LOD score of phastCons elements serves as a measure of their conservation.

2.8 | sgRNA design and plasmid construction

For single-guide RNAs (sgRNAs) design, three tools were employed: CRISPOR (http://crispor.tefor.net/),[64] CRISPR-ERA (http://crispr-era.stanford.edu/),[65] and CHOPCHOP (http://chopchop.cbu.uib.no/).[66] To ensure genome-wide sequence specificity, CRISPR Finder (https://wge.stemcell.sanger.ac.uk/)[67] and Cas-OFFinder (http://www.rgenome.net/cas-offinder/)[68] were used to examine all sgRNAs. The selection of sgRNA target sites focused on minimizing predicted off-target activity while maximizing on-target activity, employing established algorithms. In cases where the designed sgRNA sequence did not begin with a "G," a single "G" nucleotide was added at the start to enable efficient transcription from the U6 promoter. Oligonucleotides were synthesized, annealed, and cloned into the BsmBI-v2 restriction sites of the pLV-hU6-sgRNA-hUbC-dCas9-KRAB-T2a-Puro vector using the DNA Ligation Kit (Takara, Japan). The sequences of all sgRNAs can be found in Table S4.

2.9 | Lentivirus production, transduction and CRISPRi mediated repression of enhancers

To produce lentivirus, H293T cells were cultured in T175 flasks until reaching approximately 70% confluence. At this point, cells were co-transfected with 48 μg of the pLV-hU6-sgRNA-hUbC-dCas9-KRAB-T2A-Puro lentiviral expression plasmid (Addgene, #71236), 35 μg of the second-generation packaging plasmid psPAX2 (Addgene, #12260), and 12 μg of the envelope plasmid pVSV-G (Addgene, #138479) using the calcium phosphate cell transfection kit (Beyotime, China). After transfection for 8–12 h, the medium was replaced with fresh medium. Lentivirus-containing supernatants were collected at 24, 48, and 72 h post-transfection, and then filtered using Millex-HV 0.45 μm PVDF filters (Millipore, USA). The viruses were further concentrated using 100 kDa Amicon Ultra-15 centrifugal filter units (Amicon, Germany), and the titer was determined using a colloidal gold kit (Biodragon, China). The concentrated viruses were stored at −80°C.

For the infection of 3T3-L1 cells, the cells were plated in 12-well plates and allowed to adhere overnight. For each enhancer region, we designed two sgRNAs, packaged lentiviruses, and infected 3T3-L1 preadipocytes. When 3T3-L1 cells reached approximately 50–60% confluence, they were infected with 1 mL of lentivirus medium containing dCas9-KRAB-Agpat2-E1-sgRNAs, dCas9-KRAB-Agpat2-E6-sgRNAs, dCas9-KRAB-Dgat2-E2-sgRNAs, dCas9-KRAB-Dgat2-E4-sgRNAs, dCas9-KRAB-Pnpla2-E3-sgRNAs, and dCas9-KRAB-Pnpla2-E5-sgRNAs (Experimental group) or dCas9-KRAB-Control (Control group) at a multiplicity of infection (MOI) of 100 for 12 h. After 24 h post-infection, the medium was replaced. At 48 h post-infection, the cells were selected with 2 μg/mL puromycin (Sigma, USA). Through puromycin selection, stable expression of the dCas9-KRAB or dCas9-KRAB-sgRNAs system was generated in 3T3-L1 preadipocytes. The 3T3-L1 cells stably expressing dCas9-KRAB-sgRNAs or dCas9-KRAB-Control were induced for adipogenic differentiation using a standard MDI cocktail.

2.10 | Measurement of triacylglycerol content

Differentiation cells were harvested at various time points (0, 2, 7, 15, and 21 days) following lentiviral infection. TG content was determined using a colorimetric assay (Applygen, China). To remove glycerol, cells were washed twice with PBS before being lysed in the standard diluent. The mixture was split into two portions. Five hundred microliters of the mixture were centrifuged at 2000× *g* for 10 min, and the supernatant was collected. The absorbance of the dye was proportional to the concentration of TG present in each sample, and quantification of absorbance was performed at 550 nm after these reactions. The remaining portion of the mixture's protein content was measured using the BCA method. All samples were tested in duplicate, and TG values were expressed as μmol TG/g protein.

2.11 | Measurement of diacylglycerol (DAG), glycerol, phosphatidic acid (PA), lysophosphatidic acid (LPA), and free fat acid (FFA) content

Determination of intermediate product content using double antibody one-step sandwich enzyme-linked immunosorbent assay (MEIMIAN, China). Cells infected with lentivirus were collected after 7 days of differentiation. Set up standard wells and sample wells as the control group and experimental group respectively, and add 50 μL of different concentrations of standard to each control group. The sample solution to be tested is diluted with sample diluent at a ratio of 1:4. Add 100 μL of horseradish peroxidase (HRP) labeled detection antibody to each well, and incubate at 37°C in a water bath or constant temperature incubator for 1 h. Discard the liquid and wash thoroughly 5 times. Add 50 μL of substrate A and 50 μL of substrate B respectively, and incubate at 37°C in the dark for 15 min. Finally, add 50 μL of termination solution and measure the OD values of each well at a wavelength of 450 nm within 15 min to calculate the sample concentration. When using substrate TMB for color development, TMB is converted to blue under the catalysis of peroxidase and to the final yellow under the action of acid. The depth of color is positively correlated with the concentration of intermediate products in the sample.

2.12 | Preparation of Dgat2-En4 KO cells

Used three tools, CRISPOR, CRISPR-ERA, and CHOPCHOP, to design four gRNAs targeting the enhancer region. All gRNAs were checked for off-target effects using CRISPR Finder and Cas-OFFinder. After preparing the gRNAs and Cas9 protein into Cas9 RNP complexes, we electroporated them into cells and assessed their efficiency using TIDE (Tracking of Indels by Decomposition) (http://shinyapps.datacurators.nl/tide/) software. The two pairs of gRNAs with the highest cutting efficiency (gRNA1 + gRNA2 and gRNA1 + gRNA4) were selected for subsequent knockout experiments (Table S5).

The 3T3-L1 cells were seeded into T25 flasks and transfected when they reached 70–80% confluence. The cells were resuspended in an electroporation buffer at a concentration of 10^6 cells/mL. The prepared cell suspension was transferred to an electroporation cuvette, and Cas9 RNP complexes (gRNA and Cas9 protein) were added. Electroporation was performed using NEPA21 (NEPA GENE, Japan). After electroporation, a pre-warmed medium was immediately added to the cuvette to aid in cell recovery. The cells were transferred back to the T25 flask for continued culture and subsequent adipocyte differentiation.

2.13 | RNA-seq: Library preparation, sequencing, and data analysis

Total RNA was used as the starting material for RNA sample preparations. The NEBNext UltraTM RNA Library Prep Kit for Illumina (NEB, USA) was employed to generate sequencing libraries. The mRNA component was isolated from total RNA using poly-T oligo-attached magnetic beads. The resulting libraries were sequenced on the DNBSEQ-T7 platform, generating 150 bp paired-end reads. HISAT2 (v2.2.1) was utilized to align the sequence reads to the mouse reference genome (GRCm38/mm10), and quantification of gene expression was performed using featureCounts from the Rsubread package (v2.8.1). Gene expression levels for each sample were calculated as TPM values (Table). Differential analysis was conducted using DESeq2, with DEGs defined as genes having a q-value ≤.01 (Table S7). Functional enrichment analysis was carried out using Metascape, a gene annotation and analysis resource available at http://metascape.org/. GO/KEGG terms with p-values ≤.05 were considered significantly enriched. Additionally, Gene Set Enrichment Analysis (GSEA) was performed using GSEA version 4.2.3 software (https://www.gsea-msigdb.org/gsea/index.jsp) with MSigDBv7.5.1.

2.14 | Transcription factor motif enrichment analysis

To obtain the sequence data of the predicted enhancers, we retrieved the FASTA format sequences of all the enhancers from the NCBI database (https://www.ncbi.nlm.nih.gov/) using their coordinates. TF motif enrichment analysis was performed on the enhancer sequences using AnimalTFDB 3.0 (http://bioinfo.life.hust.edu.cn/AnimalTFDB#!/tfbs_predict)[69] and the JASPAR 2024 database (https://jaspar.genereg.net/).[70] The enhancer sequences were provided in FASTA format as input. Enriched TF motifs with a p-value less than .05 were identified. The sequence logos of the TF-binding site motifs were obtained from the JASPAR database.

2.15 | Statistical analysis

Statistical analyses were performed using SPSS Statistics 19.0. The data presented in the figures represent the mean ± SD and were obtained from three independent experiments unless specified otherwise. Statistical significance was determined at *$p < .05$.

3 | RESULTS

3.1 | Identification and characterization of active enhancers for key genes in TG synthesis and breakdown

TGs have a vital role in lipid droplet formation and contribute to energy storage and adipocyte differentiation. First, we investigated the stage at which five key genes involved in TG synthesis and breakdown—namely, *Agpat2*, *Dgat1*, *Dgat2*, *Pnpla2*, and *Lipe*—begin to play a role during adipocyte differentiation and lipid droplet deposition. To do this, we performed qRT-PCR at five different time points (−2 days [D-2], 2 days [D2], D4, D6, and D7 after differentiation) during the adipogenic differentiation of 3T3-L1 preadipocytes. On D2, the expression of these five genes was significantly increased ($p < .001$), and expression levels remained elevated until D7 (Figure S1A), which is in line with previous research.[10,71,72] Oil Red O and BODIPY staining were then used to evaluate the accumulation of TGs during adipocyte differentiation (Figure S1B,C). On D2, no discernible lipid staining was observed. By D7, almost the entire cellular volume exhibited staining with prominent lipid droplets, which indicates the substantial production and accumulation of TGs as well as the successful differentiation of 3T3-L1 preadipocytes (Figure S1B,C). Together, these findings suggest that these five key genes play important functional roles in adipocyte differentiation and TG metabolism.

Enhancers are crucial *cis*-regulatory elements in the eukaryotic genome and can activate gene expression in a temporal and cell-specific manner.[36,37] To identify active enhancers that regulate the expression of *Agpat2*, *Dgat1*, *Dgat2*, *Pnpla2*, and *Lipe*, we downloaded and analyzed enhancer-associated ChIP-seq and DHS-seq datasets from Day 6 and Day 7 of 3T3-L1 differentiation. Using the criteria for active enhancers described in the Section 2, we identified 24 candidate active enhancers in 3T3-L1 adipocytes, comprising six enhancers for *Agpat2*, six for

Dgat1, five for *Dgat2*, two for *Lipe*, and five for *Pnpla2* (Figures 1A and S2). BRD4 functions as an epigenetic reader, is abundant in active enhancers, and play a crucial role in adipogenesis.[73,74] MED1 is a complex subunit of the mediator complex and mediates chromatin loops between enhancers and promoters.[75,76] In ChIP-seq analysis, both proteins exhibit significant binding at regions of 24 candidate active enhancers (Figures 1A and S2). These results indicate that our candidate regions display characteristics of active enhancers.

Chromatin interactions between genes and enhancers are often located within the same TADs.[77–79] To delineate whether these five genes and their enhancers are located within the same TAD, we analyzed publicly available Hi-C data from the YUE Lab (http://3dgenome.fsm.northwestern.edu/). Given that TAD boundaries are typically conserved across cell types within the same species,[77,80–83] we depicted the TADs of these genes in five different cell types in mice, as illustrated in Figures 1A and S3. The 24 identified candidate enhancers and their target genes were located within the same TAD, exhibiting pronounced chromatin interactions (Figures 1A and S3). These results suggest that the identified candidate enhancers and genes reside within a shared interacting domain.

To experimentally assess the activity of these candidate enhancers, we conducted enhancer dual-luciferase reporter gene assays in differentiated adipocytes. Eleven of the 24 enhancers (Agpat2-En1, Agpat2-En2, Agpat2-En5, Agpat2-En6, Dgat1-En1, Dgat2-En2, Dgat2-En4, Lipe-En1, Lipe-En2, Pnpla2-En3, and Pnpla2-En5) exhibited significantly higher luciferase activity ($p < .05$) than the PGL3-promoter control group in differentiated adipocytes (Figure 1B). Moreover, Agpat2-En6, Dgat1-En1, Dgat2-En2, Pnpla2-En5, and Lipe-En1 had the highest transcriptional activity among the enhancers for the respective target genes (Figure 1B). Of these, Lipe-En1 exhibited the strongest transcriptional activity, with a 5.44-fold increase in luciferase activity compared with the pGL3-promoter vector. To assess the potential impact of differentiation on the expression of active enhancers for these five genes, we further performed luciferase reporter gene assays to examine their activity during the differentiation process of 3T3-L1 adipocytes. Among the 24 enhancers, 13 (Agpat2-En1, Agpat2-En2, Agpat2-En5, Dgat1-En1, Dgat1-En2, Dgat1-En4, Dgat1-En6, Dgat2-En2, Lipe-En1, Lipe-En2, Pnpla2-En1, Pnpla2-En3, and Pnpla2-En5) exhibited significantly higher luciferase activity ($p < .05$) in 3T3-L1 preadipocytes compared to the pGL3 promoter control group (Figure S4). From D2 to D7 of differentiation, enhancer activity showed dynamic changes (Figure S4). This suggests that active enhancers potentially regulate gene expression in a stage-specific manner during differentiation. The increase in activity after differentiation,

coupled with the differential activity of these enhancers between 3T3-L1 preadipocytes and adipocytes, indicates that they exert distinct regulatory effects on the expression of *Agpat2*, *Dgat1*, *Dgat2*, *Pnpla2*, and *Lipe*, with these effects varying throughout the differentiation process.

Enhancers exhibit evolutionarily conserved sequence properties.[84,85] We characterized the sequence conservation of these active enhancers across species. Of the 11 active enhancers, we observed that seven contained at least one conserved element (Figures 1C and S5), as measured by log-odds ratio scores from the phastCons program. Pnpla2-En3, Agpat2-En1, Dgat1-En1, Dgat2-En2, and Lipe-En2 displayed the highest levels of conservation within their respective gene sequences (Figures 1C and S5). Together, these results suggest that the majority of the identified active enhancers exhibit a degree of evolutionary conservation. Studies have found that approximately 90% of the identified genetic variations are located in non-coding regions, including enhancers.[86] These genetic variation sites and their association with phenotypes are widely used to identify gene loci related to traits and diseases.[87–89] Investigating whether genetic variations at enhancers is therefore highly valuable. In this study, we used the Ensembl database (https://useast.ensembl.org/index.html) to perform single-nucleotide polymorphism (SNP) detection in active enhancers and assess their association with phenotype-related signals. The results showed that SNPs were present in all 11 active enhancer regions (Figure S6A,B). Notably, Lipe-En1 and Lipe-En2 were found to be associated with disease phenotypes, including lipid homeostasis abnormalities, reduced susceptibility to diet-induced obesity, and insulin resistance (Figure S6A). In conclusion, we conducted a comprehensive assessment of the transcriptional activity and characteristics of the candidate active enhancers.

3.2 | Inhibition of *Agpat2* and *Dgat2* enhancers reduces target gene expression and suppresses TG accumulation

To investigate the role of these active enhancers in the regulation of target gene expression, we used the CRISPRi (dCas9-KRAB) system to target the two enhancers with the highest fluorescence activity in *Agpat2* and *Dgat2*, with two sgRNAs designed for each enhancer (Figure S7A). The dCas9-KRAB system is a modified CRISPR/Cas9 genome-editing technology that uses a deactivated Cas9 fused to the repressor KRAB to repress gene transcription.[90,91] We used qRT-PCR to assess *Agpat2* and *Dgat2* expression levels before and after differentiation (Figure 2A,B). At D-2, the repression of Agpat2-En1 or -En6 regions did not

(A)
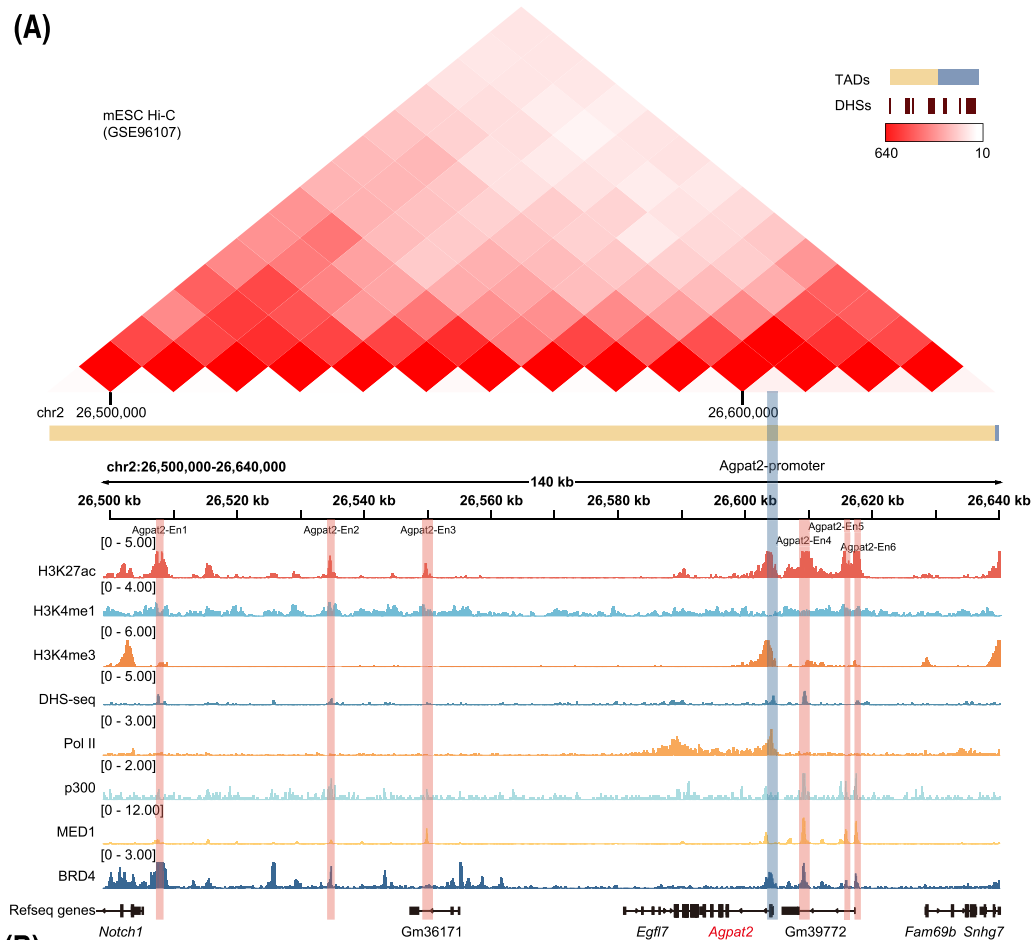
(B)
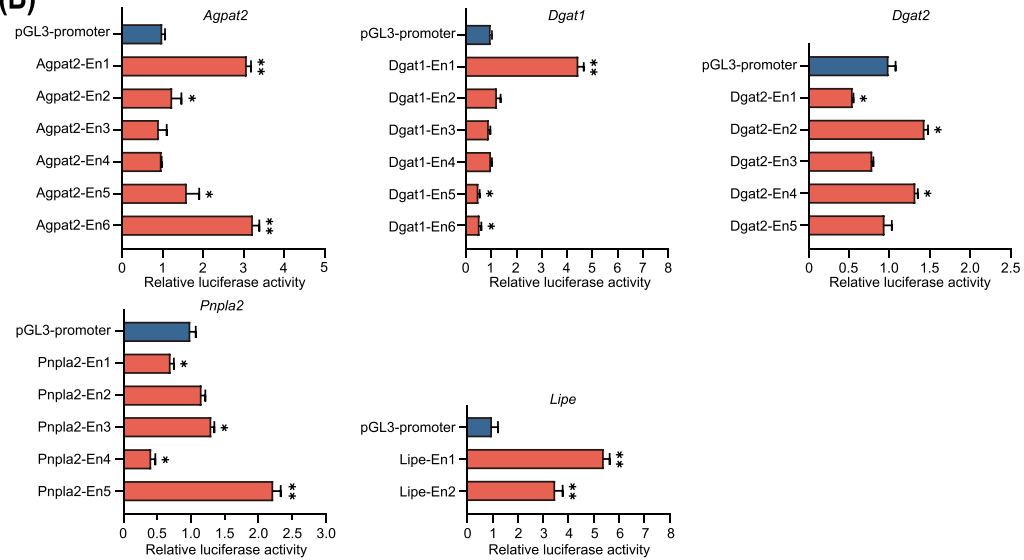
(C)
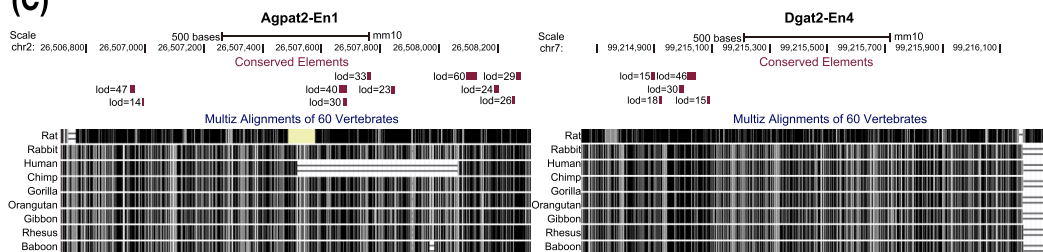
FIGURE 1 Identification of candidate enhancers for the key genes involved in TG synthesis and breakdown in 3T3-L1 adipocytes. (A) Identification of candidate enhancers for *Agpat2* in 3T3-L1 adipocytes. Top panel: Hi-C heatmap derived from mouse embryonic stem cells (mESCs) displaying six enhancers for *Agpat2* and its promoter within the same interaction domain. Bottom panel: ChIP-seq profiles for H3K27ac, H3K4me1, H3K4me3, BRD4, MED1, p300, and RNA Pol II marked in 3T3-L1 adipocytes, along with DHS-seq profiles for the *Agpat2* gene locus in 3T3-L1 adipocytes. Red bars represent *Agpat2* enhancers and green bars represent *Agpat2* promoters. (B) Luciferase reporter assays of candidate enhancers. The pGL3-promoter-enhancer vector was transfected into 3T3-L1 cells that were differentiated for 4 days; luciferase activity was measured 2 days post-transfection. The pGL3-promoter was used as a control. Luciferase signals were normalized to Renilla luciferase signals. (C) Sequence conservation analysis of Agpat2-En1 and Dgat2-En4 in the selected species was conducted using the UCSC Genome Browser. Horizontal red bars represent conserved elements in placental mammals. Element conservation was quantified as the logarithm of the ratio score of phastCons program elements. Data are expressed as the mean $\pm$ SD of three independent experiments, and *p*-values were calculated using the Wilcoxon Ranksum test (*$p < .05$, **$p < .01$).

significantly alter *Agpat2* expression compared with the dCas9-KRAB control (Figure 2A). Similarly, compared with the control group, the groups in which Dgat2-En2 or -En4 regions were repressed did not show a significant change in *Dgat2* expression (Figure 2B). From D2 to D7, groups in which Agpat2-En1 or -En6 and Dgat2-En2 or -En4 regions were inhibited showed significant reductions ($p < .05$) in *Agpat2* and *Dgat2* expression, respectively, compared with the control group. It was also noteworthy that Agpat2-En1 repression resulted in a more pronounced downregulation of *Agpat2* mRNA expression than Agpat2-En6 repression at D7 (Figure 2A). Similarly, compared with that of Dgat2-En2, the repression of Dgat2-En4 led to a greater reduction in *Dgat2* expression (Figure 2B). Thus, the suppression of these four enhancers individually led to impairments in *Agpat2* and *Dgat2* expression. These results indicate that Agpat2-En1, Agpat2-En6, Dgat2-En2, and Dgat2-En4 functionally regulate the expression of their target genes during adipogenic differentiation.

To investigate whether these functional enhancers influence TG synthesis and adipocyte differentiation, we conducted a study on dCas9-KRAB-Agpat2-En1, dCas9-KRAB-Agpat2-En6, dCas9-KRAB-Dgat2-En2, and dCas9-KRAB-Dgat2-En4 cells on D7. First, we used qRT-PCR to detect the expression of key genes involved in lipid metabolism and adipocyte proliferation. Compared with the dCas9-KRAB control group, groups in which Agpat2-En1, Agpat2-En6, Dgat2-En2, and Dgat2-En4 were repressed showed significantly ($p < .05$) reduced expression of *Fabp4*, *Lpl*, *Adipoq*, *Slc2a4*, *Cebpa*, *Pparg*, and *Fasn* (Figure S7B,C). Next, we performed BODIPY staining on dCas9-KRAB control, dCas9-KRAB-Agpat2-En1, dCas9-KRAB-Agpat2-En6, dCas9-KRAB-Dgat2-En2, and dCas9-KRAB-Dgat2-En4 cells on D7. Compared with the control, the repression of Agpat2-En1, Agpat2-En6, Dgat2-En2, and Dgat2-En4 reduced intracellular lipid droplet deposition, thus inhibiting adipocyte differentiation (Figure 2C). Additionally, TG measurements demonstrated that inhibiting Agpat2-En1, Agpat2-En6,

Dgat2-En2, and Dgat2-En4 significantly reduced ($p < .05$) TG deposition (Figure 2D,E). Notably, at D21, the intracellular TG contents of dCas9-KRAB-Agpat2-En1 and dCas9-KRAB-Dgat2-En4 cells were 44.83% and 35.42% lower, respectively, than that of the control group. Additionally, in the cells with inhibited Agpat2-En6, both LPA and PA levels were significantly ($p < .05$) increased (Figure S7D); whereas, inhibition of Dgat2-En4 led to a significant ($p < .05$) decrease in DAG levels (Figure S7E). These findings indicate that Agpat2-En1, Agpat2-En6, Dgat2-En2, and Dgat2-En4 play a role in regulating lipid droplet formation and adipocyte differentiation. To validate whether changes in lipid metabolism during adipocyte differentiation affect not only TG but also other lipid processes, we measured the levels of FFA, PA, LPA, and glycerol in 3T3-L1 cells on Day 7 of differentiation, following the inhibition of Agpat2-En6 and Dgat2-En4. The results, shown in Figure S7D,E indicate that inhibition of Agpat2-En6 leads to a significant increase ($p < .05$) in PA, LPA, and FFA levels, with no significant change in glycerol content (Figure S7D). In contrast, inhibition of Dgat2-En4 significantly decreased ($p < .05$) the levels of PA, LPA, FFA, and glycerol (Figure S7E). These findings suggest that inhibiting enhancers can affect lipid metabolic pathways.

To investigate whether functional enhancers directly influence target gene expression and adipocyte differentiation, we performed an enhancer knockout experiment for Dgat2-En4 in 3T3-L1 cells. First, we successfully established a Dgat2-En4 knockout 3T3-L1 cell line (Figure S8A–D). We then assessed the expression of the *Dgat2* target gene on D7 of differentiation using qRT-PCR. Compared to wild-type (WT) 3T3-L1 cells, the Dgat2-En4-KO group exhibited a significant downregulation of *Dgat2* expression ($p < .01$), indicating that the activity of Dgat2-En4 directly regulates *Dgat2* expression (Figure 2F). Furthermore, compared to the WT group, the Dgat2-En4-KO group showed a significant reduction ($p < .05$) in the expression of *Fabp4*, *Lpl*, *Adipoq*, *Slc2a4*, *Cebpa*, and *Pparg* (Figure 2G). We performed Oil Red O and BODIPY staining on Dgat2-En4-KO and WT cells on
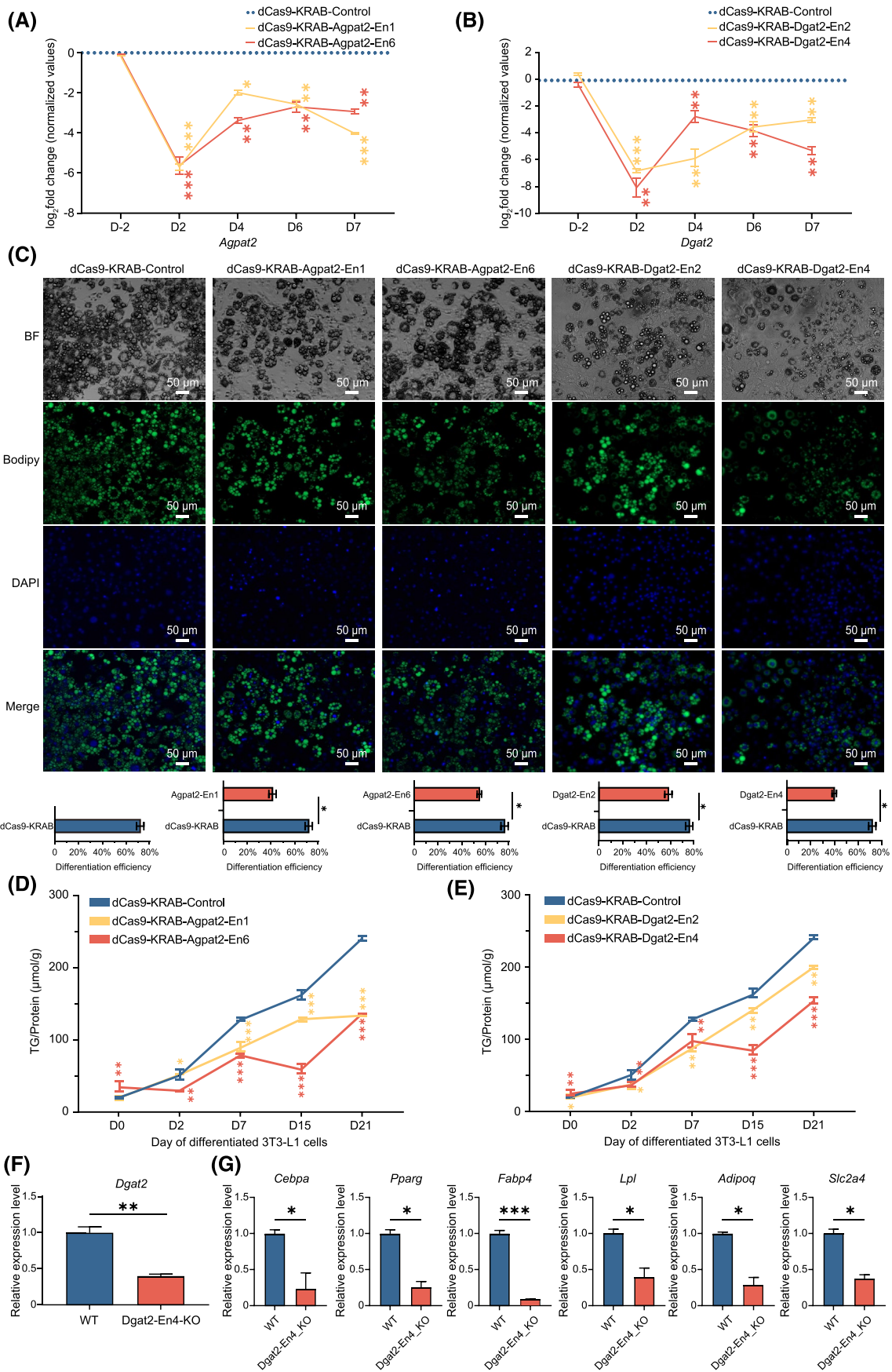
FIGURE 2 Inhibition of enhancers for *Agpat2* and *Dgat2* affects TG accumulation. (A and B) Log$_2$ fold changes in the expression of *Agpat2* (A) and *Dgat2* (B) in dCas9-KRAB-Agpat2-En1, dCas9-KRAB-Agpat2-En6, dCas9-KRAB-Dgat2-En2, and dCas9-KRAB-Dgat2-En4 cells compared with the expression in dCas9-KRAB control cells were determined by qRT-PCR at D-2, D2, D4, D6, and D7. The blue dashed line represents a log$_2$ fold change of 0. Error bars correspond to ±1 SD. Significant differences in expression ($p < .05$, two-sided Welch one-sample *t*-test with Bonferroni correction for multiple testing) are indicated by asterisks. (C) On D7, BODIPY (green) staining for lipid droplets and DAPI (blue) staining were performed in 3T3-L1 adipocytes transduced with dCas9-KRAB-Agpat2-En1, dCas9-KRAB-Agpat2-En6, dCas9-KRAB-Dgat2-En2, and dCas9-KRAB-Dgat2-En4. Cell differentiation efficiency was determined by counting cells in five randomly selected microscopic fields for both dCas9-KRAB and dCas9-KRAB-sgRNA cells; BF, bright field. (D and E) Compared with that in the dCas9-KRAB control, TG content was assessed at different time points during the differentiation process in 3T3-L1 cells transduced with dCas9-KRAB-Agpat2-En1 and dCas9-KRAB-Agpat2-En6 (D), dCas9-KRAB-Dgat2-En2 and dCas9-KRAB-Dgat2-En4 (E). Cellular TG content was normalized to total protein levels. Wilcoxon Ranksum test was used to calculate *p*-values (*$p < .05$, **$p < .01$, ***$p < .001$). (F) Expression of *Dgat2* in WT and Dgat2-En4-KO cells was determined by qRT-PCR at D7. Bars show the mean and SD ($n = 3$; **$p < .01$). (G) At D7, qRT-PCR analysis of key genes involved in lipid metabolism and adipocyte differentiation was conducted in WT and Dgat2-En4-KO cells. Bars show the mean and SD ($n = 3$; *$p < .05$, **$p < .01$, ***$p < .001$).

Day 7 of differentiation. The results showed that lipid droplet deposition was reduced in the Dgat2-En4-KO group (Figure S8E,F). These findings suggest that Dgat2-En4 directly regulates the expression of *Dgat2* and plays a role in regulating adipocyte differentiation.

3.3 | Inhibition of Dgat2-En4 alters the TG metabolism pathway in adipocytes

DGAT2 functions as the rate-limiting enzyme in the final step of TG synthesis. To further investigate the impact of Dgat2-En4 enhancer inhibition on TG metabolism and adipocyte differentiation, we conducted a transcriptome analysis of dCas9-KRAB-Dgat2-En4 and dCas9-KRAB cells on D7. The RNA-seq analysis revealed a high degree of correlation between replicate samples in dCas9-KRAB-Dgat2-En4 and dCas9-KRAB cells (Figure 3A). Furthermore, samples from the same groups clustered together, whereas those from different groups were separate (Figure 3B). This finding indicates the existence of distinct expression patterns between dCas9-KRAB-Dgat2-En4 cells and the control group.

Differential expression analysis identified 2184 differentially expressed genes (DEGs), comprising 734 downregulated DEGs and 1450 upregulated DEGs, in dCas9-KRAB-Dgat2-En4 cells (Figure 3C, Table S7). Compared with that in the control group, *Dgat2* expression was significantly decreased ($p < .01$) in dCas9-KRAB-Dgat2-En4 cells, consistent with the qRT-PCR results (Figure 3D). To determine the impact of Dgat2-En4 inhibition on biological processes and pathways in 3T3-L1 adipocytes, we performed a functional enrichment analysis of the DEGs using Metascape. The downregulated DEGs in dCas9-KRAB-Dgat2-En4 cells were significantly enriched in terms such as oxidoreductase activity, fatty acid metabolic process, fat cell differentiation, and the PPAR signaling pathway (Figure 3E). In addition, multiple

processes related to lipid droplets, including lipid catabolic process, lipid biosynthetic process, and neutral lipid metabolic process, were significantly enriched (Figure 3E). Compared with those in the control cells, genes related to TG biosynthesis were significantly downregulated in dCas9-KRAB-Dgat2-En4 cells, including *Dgat1*, *Acsl1*, *Agpat2*, and *Dgat2* (Figure 3F). Consistent with the enrichment results from Metascape, gene set enrichment analysis (GSEA) of expression genes revealed significant enrichments in cellular lipid catabolic processes, fatty acid metabolism, and regulation of lipid biosynthetic processes in dCas9-KRAB cells compared with the findings in dCas9-KRAB-Dgat2-En4 cells (Figure 3G). Moreover, glycerolipid biosynthesis processes were notably enriched in dCas9-KRAB cells (Figure 3G). Together, these results suggest that Dgat2-En4 inhibition alters the transcriptome of adipocytes, thus suppressing TG synthesis, adipocyte differentiation, and lipid biosynthetic pathways. These findings underscore the crucial role of Dgat2-En4 in the transcriptional regulation and adipogenesis of *Dgat2*, and in lipid generation.

3.4 | Pnpla2-En5 regulate *Pnpla2* expression and TG breakdown

To explore the role of *Pnpla2* enhancers in regulating *Pnpla2* expression, we designed two sgRNAs for each enhancer and used the CRISPRi system to target the enhancers with the highest fluorescence activity within the *Pnpla2* locus, which was Pnpla2-En3 and Pnpla2-En5 (Figure S9A). Changes in *Pnpla2* expression levels were then assessed by qRT-PCR before and after differentiation. On D-2, cells in which Pnpla2-En3 and -En5 regions were inhibited did not show significantly ($p > .05$) altered *Pnpla2* expression compared with control cells (Figure 4A). However, from D2 to D7, cells in which Pnpla2-En3 and Pnpla2-En5 regions were suppressed showed a significant
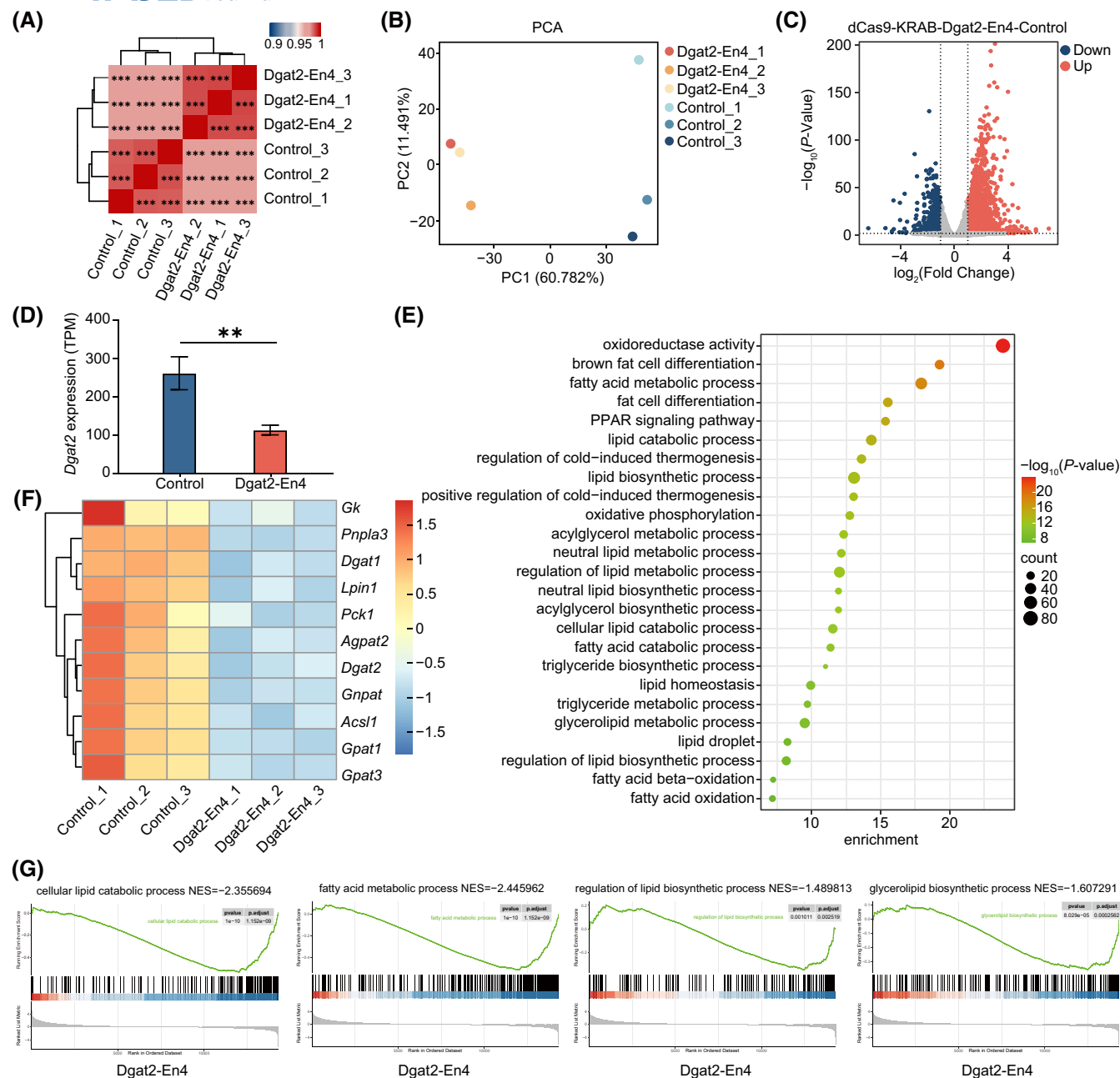
FIGURE 3 Inhibition of Dgat2-En4 and its impact on the transcriptional profile during TG metabolism. (A) Heatmap showing hierarchical clustering of Pearson's correlation scores between samples of dCas9-KRAB-Dgat2-En4 and dCas9-KRAB control cells ($n = 3$; ***$p < .001$). (B) Principal component analysis (PCA) plot of normalized RNA-seq data for dCas9-KRAB-Dgat2-En4 and dCas9-KRAB control cells, represented as transcripts per million (TPM). The percentage shown on each axis represents the variation explained by the principal component. (C) Volcano plot depicting the DEGs (|$\log_2$(FoldChange)|≥ 1 and q-value $\leq .01$) between dCas9-KRAB and dCas9-KRAB-Dgat2-En4 cells. Blue and red dots represent downregulated and upregulated DEGs, respectively, in dCas9-KRAB-Dgat2-En4 versus dCas9-KRAB cells. (D) Expression levels of *Dgat2* in dCas9-KRAB and dCas9-KRAB-Dgat2-En4 cells, measured in TPM. Bars show the mean and SD ($n = 3$; **$p < .01$). (E) Functional enrichment analysis of downregulated DEGs in dCas9-KRAB-Dgat2-En4 cells was performed using Metascape. The dot size represents the number of genes, and the color bar represents the $-\log_{10}$(p-value). (F) Heatmap displaying gene expression levels (z-scores) in dCas9-KRAB and dCas9-KRAB-Dgat2-En4 cells. Genes are hierarchically clustered. (G) GSEA was conducted for all expressed genes in dCas9-KRAB control and dCas9-KRAB-Dgat2-En4 cells. Positive normalized enrichment scores (NES) indicate enrichment in dCas9-KRAB cells, whereas negative values indicate enrichment in dCas9-KRAB-Dgat2-En4 cells.

decrease in *Pnpla2* expression compared with control cells (Figure 4A). These results indicate that Pnpla2-En3 and Pnpla2-En5 dynamically regulate *Pnpla2* expression

during adipogenic differentiation. It was also noteworthy that, on D7, the downregulation of *Pnpla2* was more pronounced in dCas9-KRAB-Pnpla2-En5 cells than in

dCas9-KRAB-Pnpla2-En3 cells (Figure 4A). Together, these findings suggest the functional regulatory role of Pnpla2-En3 and Pnpla2-En5 in modulating *Pnpla2* expression.

To elucidate whether Pnpla2-En3 and Pnpla2-En5 affect TG metabolism, we conducted further studies using dCas9-KRAB-Pnpla2-En3 and dCas9-KRAB-Pnpla2-En5 cells on D7. BODIPY staining was performed on D7 for dCas9-KRAB control, dCas9-KRAB-Pnpla2-En3, and dCas9-KRAB-Pnpla2-En5 cells. Compared with control cells, cells with Pnpla2-En5 inhibition exhibited enhanced lipid droplet formation (Figure 4B); the inhibitory effect of Pnpla2-En3 was less pronounced than that of Pnpla2-En5. Subsequently, we used ImageJ software to quantify lipid droplet diameter, area, and overall size distribution in control, dCas9-KRAB-Pnpla2-En3 and dCas9-KRAB-Pnpla2-En5 cells. Compared with the control group, dCas9-KRAB-Pnpla2-En5 cells showed an increase in the number of lipid droplets with a diameter of 10–30 μm, while the number of lipid droplets with a diameter of 0–5 μm decreased (Figure 4C). These results suggest that inhibition of Pnpla2-En5 activity leads to lipid droplet accumulation, with an increase in large droplets and a decrease in small droplets. Furthermore, we observed the average lipid droplet area per differentiated cell in the field of view; the average lipid droplet area was significantly larger in dCas9-KRAB-Pnpla2-En3 and dCas9-KRAB-Pnpla2-En5 cells compared to the control group (Figure 4D). Measurements of TG content on Day 21 showed that TG deposition significantly ($p < .05$) increased in cells with Pnpla2-En5 inhibition compared to control cells and inhibition of Pnpla2-En3 also led to a significant increase in TG levels (Figure 4E), although the increase was less pronounced than that observed with Pnpla2-En5 inhibition. At the same time, the levels of DAG and FFA in the cells on D7 of differentiation were measured, and it was found that both DAG and FFA levels were significantly decreased compared to the control group (Figure S9B). Together, these findings suggest that Pnpla2-En3 and Pnpla2-En5 influence lipid droplet formation and TG deposition. To investigate whether changes in lipid metabolism during adipocyte differentiation also affect other lipid processes, we measured the levels of FFA, PA, LPA, and glycerol in 3T3-L1 cells on D7 of differentiation following inhibition of Pnpla2-En5. The results, as shown in Figure S9B, indicated that while PA levels remained unchanged, the levels of FFA, LPA, and glycerol were significantly decreased in the Pnpla2-En5-inhibited cells. These findings suggest that inhibition of Pnpla2-En5 affects lipid metabolism pathways.

To further investigate the impact of inhibiting the functionally potent enhancer Pnpla2-En5 on TG metabolism, we performed RNA-seq on dCas9-KRAB-Pnpla2-En5 cells

on D7. There were significant differences in expression patterns between dCas9-KRAB-Pnpla2-En5 and control cells, as evidenced by the high correlations observed among replicate samples within dCas9-KRAB-Pnpla2-En5 and dCas9-KRAB cells (Figure S9C); samples from the same group clustered together, whereas those from different groups were separate (Figure S9D). Of the 1416 DEGs that were identified in the differential expression analysis, 452 were downregulated and 964 were upregulated (Figure 4G, Table S7). To discern the impact of Pnpla2-En5 inhibition on biological processes and pathways in 3T3-L1 adipocytes, functional enrichment analysis was conducted on the downregulated genes in dCas9-KRAB-Pnpla2-En5 cells using Metascape. There was a significant enrichment of terms related to oxidation–reduction, lipid droplet metabolism, and TG metabolism (Figure 4H). Enriched terms also included the PPAR signaling pathway and TG metabolic processes. Furthermore, consistent with the enrichment results from Metascape, GSEA analysis of dCas9-KRAB-Pnpla2-En5 cells compared with dCas9-KRAB cells revealed significant enrichment in the regulation of lipid metabolism processes, cellular lipid catabolic processes, and lipid catabolic processes (Figure 4I). Together, these results suggest that Pnpla2-En5 inhibition alters the transcriptome of adipocytes, thus suppressing TG metabolism and lipid metabolic pathways. They also indicate the potentially critical role of Pnpla2-En5 in the transcriptional regulation of *Pnpla2* and in TG hydrolysis.

3.5 | PPARG and RXRA regulate Agpat2-En1, Dgat2-En4, and Pnpla2-En5 activity

TFs can regulate enhancer activity by binding to specific DNA sequences and can influence gene expression through chromatin interactions between enhancers and promoters.[49,92] To investigate the TFs that regulate enhancer activity, we performed TF prediction analysis for the three functionally strongest enhancers using AnimalTFDB 3.0[69] and JASPAR 2024. We revealed that 96 commonly predicted TFs bind to Agpat2-En1, 103 TFs bind to Dgat2-En4, and 108 TFs bind to Pnpla2-En5 (Table S8). Of these, PPARG, CEBPA, RXRA, KLF4, PPARA, and SREBF1 were co-predicted to bind to these three enhancers, and these TFs possessed high prediction scores (Figure 5A). Furthermore, previous studies have indicated that these TFs are involved in the processes of TG metabolism and adipocyte differentiation—especially PPARG,[93,94] RXRA,[95] and CEBPA.[57] Next, we retrieved ChIP-seq data for PPARG, RXRA, and CEBPA from CistromeDB (http://cistrome.org/db/#/) and analyzed their enrichment in the Agpat2-En1, Dgat2-En4, and

(A) dCas9-KRAB-Control, dCas9-KRAB-Pnpla2-En3, dCas9-KRAB-Pnpla2-En5

(B) dCas9-KRAB-Control, dCas9-KRAB-Pnpla2-En3, dCas9-KRAB-Pnpla2-En5; BF, DAPI, Bodipy, Merge

(C) dCas9-KRAB-Control, dCas9-KRAB-Pnpla2-En3, dCas9-KRAB-Pnpla2-En5

(D) Average size of Lipid droplet (μm²)

(E) TG/Protein (μmol/g); Day of differentiated 3T3-L1 cells

(F) Pnpla2 expression (TPM)

(G) dCas9-KRAB-Pnpla2-En5-Control; Down, Up

(H) PPAR signaling pathway, regulation of lipolysis in adipocytes, oxidative phosphorylation, fatty acid metabolic process, lipid biosynthetic process, glycerolipid metabolic process, triglyceride metabolic process, AMPK signaling pathway, cellular lipid catabolic process, regulation of lipid metabolic process, fatty acid catabolic process, negative regulation of lipid catabolic process, regulation of lipid catabolic process, adipocytokine signaling pathway, lipid homeostasis

(I) cellular lipid catabolic process NES=−2.085772; lipid catabolic process NES=−1.979251; regulation of lipid metabolic process NES=−1.399442

FIGURE 4 Inhibition of Pnpla2-En3 and Pnpla2-En5 affects *Pnpla2* expression and TG metabolism. (A) Log$_2$ fold changes in *Pnpla2* expression in dCas9-KRAB-Pnpla2-En3 and dCas9-KRAB-Pnpla2-En5 cells compared with that in dCas9-KRAB control cells were determined by qRT-PCR at D-2, D2, D4, D6, and D7. The blue dashed line represents a log$_2$ fold change of 0. Error bars correspond to ±1 SD. Significant differences in expression ($p < .05$, two-sided Welch one-sample t-test with Bonferroni correction for multiple testing) are indicated by asterisks. (B) On D7, BODIPY (green) staining for lipid droplets and DAPI (blue) staining were performed in 3T3-L1 adipocytes transduced with dCas9-KRAB-Pnpla2-En3 and dCas9-KRAB-Pnpla2-En5; BF, bright field. (C) Distribution of lipid droplets in the dCas9-KRAB control, dCas9-KRAB-Pnpla2-En3, and dCas9-KRAB-Pnpla2-En5 cells measured using ImageJ software. Data were collected from at least 2000 lipid droplets. (D) Average size of lipid droplets per cell in the dCas9-KRAB control, dCas9-KRAB-Pnpla2-En3, and dCas9-KRAB-Pnpla2-En5 cells. Sixty to seventy cells per group were used for the measurements. Wilcoxon Ranksum test was used to calculate p-values ($*p < .05$, $**p < .01$). (E) Compared with that in dCas9-KRAB control cells, the TG content was assessed at different time points during the differentiation process in 3T3-L1 cells transduced with dCas9-KRAB-Pnpla2-En3 and dCas9-KRAB-Pnpla2-En5. Cellular TG content was normalized to total protein levels. (F) Expression levels (TPM) of *Pnpla2* in dCas9-KRAB and dCas9-KRAB-En5 cells. Bars show the mean and standard deviation ($n = 3$); $**p < .01$. (G) Volcano plot depicting the DEGs (q-value ≤.01) between dCas9-KRAB and dCas9-KRAB-Pnpla2-En5 cells. Blue and red dots represent downregulated and upregulated DEGs, respectively, in dCas9-KRAB-Pnpla2-En5 versus dCas9-KRAB cells. (H) Functional enrichment analysis of downregulated DEGs in dCas9-KRAB-Pnpla2-En5 cells was performed using Metascape. The dot size represents the number of genes, and the color bar represents the $-\log_{10}(p\text{-value})$. (I) GSEA was conducted for all expressed genes in dCas9-KRAB control and dCas9-KRAB-Pnpla2-En5 cells. Positive NES values indicate enrichment in dCas9-KRAB cells, whereas negative values indicate enrichment in dCas9-KRAB-Pnpla2-En5 cells.

Pnpla2-En5 regions in 3T3-L1-AD. There was significant enrichment of PPARG in the Agpat2-En1, Dgat2-En4, and Pnpla2-En5 regions. Additionally, RXRA exhibited lower but significant enrichment in these enhancer regions, whereas CEBPA had the least enrichment in these enhancer regions (Figure 5B). These results suggest that PPARG and RXRA might be involved in the regulation of Agpat2-En1, Dgat2-En4, and Pnpla2-En5 activity.

To evaluate the impact of PPARG and RXRA on the aforementioned enhancer activity, we conducted luciferase reporter assays by overexpressing PPARG or RXRA in H293T cells. Compared with pEGFP-N1 plasmid transfection, the individual overexpression of PPARG or RXRA significantly increased ($p < .05$) Agpat2-En1, Dgat2-En4, and Pnpla2-En5 activity (Figure 5C). Furthermore, compared with PPARG overexpression, RXRA overexpression resulted in higher fluorescence activity in Agpat2-En1, Dgat2-En4, and Pnpla2-En5 (Figure 5C), suggesting that RXRA has a stronger enhancer activity regulatory capacity than PPARG. Together, these results indicate that PPARG and RXRA binding can enhance the transcriptional activity of Agpat2-En1, Dgat2-En4, and Pnpla2-En5.

To further investigate whether the critical binding sites of PPARG and RXRA TFs affect Agpat2-En1, Dgat2-En4, and Pnpla2-En5 activity, we performed a motif analysis of TF binding sites using the JASPAR 2024 and AnimalTFDB 3.0 databases. Three common binding sites for the PPARG and RXRA TFs were predicted within the sequences of Agpat2-En1, Dgat2-En4, and Pnpla2-En5, denoted as Agpat2-En1-motif, Dgat2-En4-motif, and Pnpla2-En5-motif, respectively (Figure 5D). Subsequently, we constructed deletion mutants for each binding site in the pGL3-promoter-Ens plasmids (Figure 5E) and conducted luciferase reporter gene assays in H293T cells co-transfected with overexpression plasmids for RXRA

or PPARG. Upon co-transfection with the PPARG overexpression plasmid, mutations in the Agpat2-En1-motif and Dgat2-En4-motif significantly decreased ($p < .05$) Agpat2-En1 and Dgat2-En4 activity, whereas the mutation in Pnpla2-En5-motif had no significant effect on Pnpla2-En5 activity (Figure 5F). Upon co-transfection with the RXRA overexpression plasmid, the impact of mutations in the Agpat2-En1-motif, Dgat2-En4-motif, and Pnpla2-En5-motif on Agpat2-En1, Dgat2-En4, and Pnpla2-En5 activity were in line with the results obtained with the PPARG overexpression plasmid (Figure 5G). These findings suggest that RXRA and PPARG play crucial roles in regulating Agpat2-En1 and Dgat2-En4 activity by binding their respective motifs. Overall, our data indicate that the binding of PPARG and RXRA to Agpat2-En1, Dgat2-En4, and Pnpla2-En5 plays a critical role in regulating target gene expression.

4 | DISCUSSION

TGs are the main form of energy storage in higher eukaryotes.[96] The aberrant synthesis and degradation of TGs can lead to metabolic dysregulation, influence adipose tissue development, and contribute to the occurrence of metabolic diseases,[97] this underscores the crucial importance of maintaining a balanced TG metabolism for the growth and development of organisms. In vivo, TG metabolism is intricately regulated by a series of synthetic and degradative enzymes. Among these enzymes, the precise expression of AGPAT2, DGAT1, DGAT2, ATGL, and HSL is crucial for the regulation of TG metabolism.

In eukaryotic organisms, gene expression is finely regulated to maintain tissue function, with temporal and spatial specificity.[98] Transcriptional regulation, involving
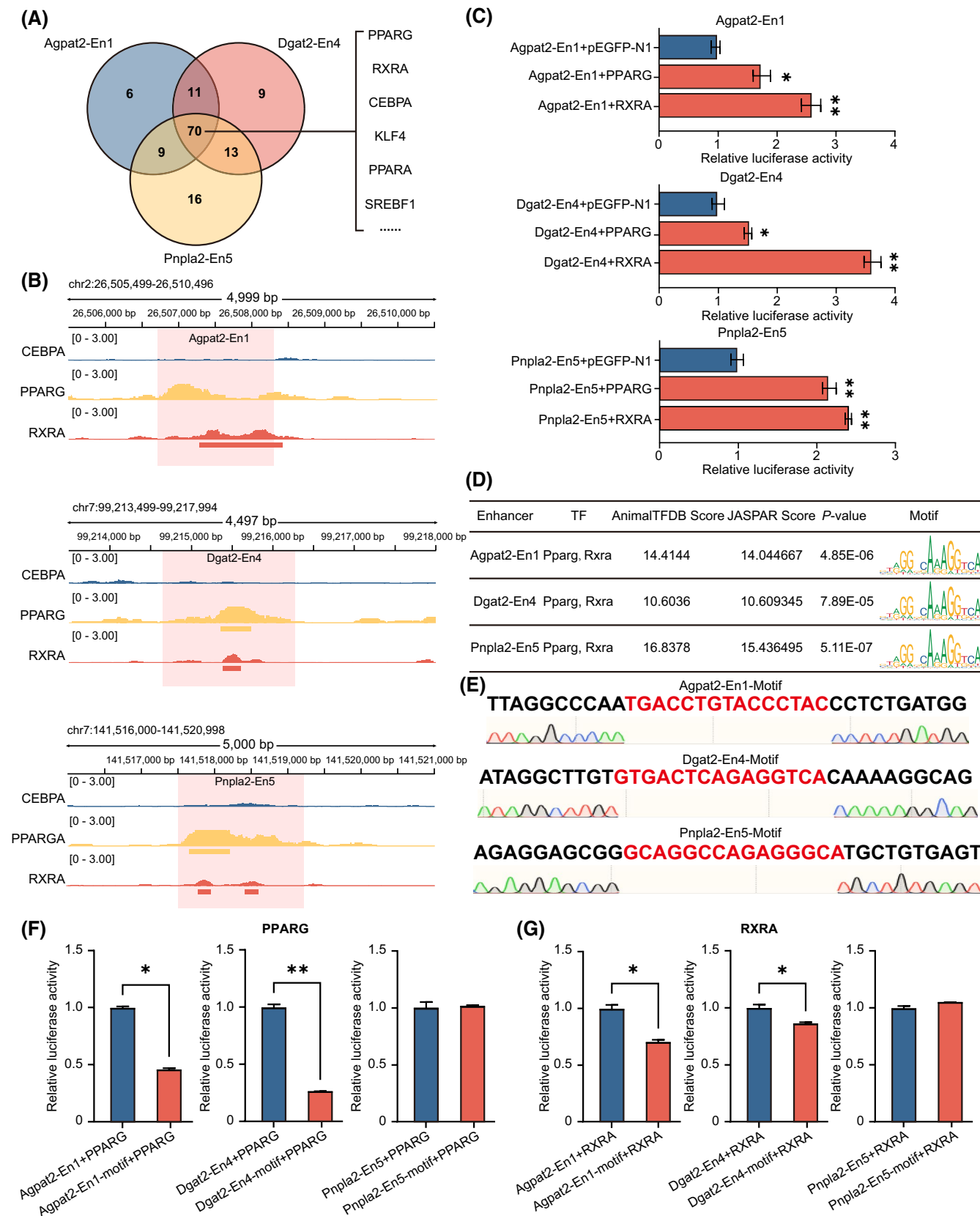
enhancers,[99] promoters,[100] transcription factors,[101] and miRNAs,[102] controls various steps in the transcription process. For instance, carbohydrate response element binding protein (ChREBP) binds to the human *Dgat2* promoter in a glucose-dependent manner, activating *Dgat2* promoter activity. SP1, as a co-regulatory factor of

FIGURE 5 Regulation of Agpat2-En1, Dgat2-En4, and Pnpla2-En5 activity by RXRA and PPARG. (A) Venn diagram showing the comparison of shared and unique TFs identified from the enhancer regions Agpat2-En1, Dgat2-En4, and Pnpla2-En5 between AnimalTFDB 3.0 and JASPAR 2024. (B) ChIP-seq profiles depicting the enrichment patterns of CEBPA, PPARG, and RXRA in the regions of Agpat2-En1, Dgat2-En4, and Pnpla2-En5. (C) In H293T cells, the relative luciferase activity of Agpat2-En1, Dgat2-En4, and Pnpla2-En5 was assessed after overexpressing PPARG or RXRA. Data are presented as the mean $\pm$ SD from three independent experiments. (D) Enrichment analysis of the common binding sites of PPARG and RXRA in the regions of Agpat2-En1, Dgat2-En4, and Pnpla2-En5. (E) Schematic diagram illustrating the motif sequences of predicted common binding sites for PPARG and RXRA in the regions of Agpat2-En1, Dgat2-En4, and Pnpla2-En5. Confirmation of deletion mutations for each motif through Sanger sequencing is also shown. (F and G) In H293T cells, the relative luciferase activity of regions Agpat2-En1, Dgat2-En4, and Pnpla2-En5 carrying mutations in common binding sites of PPARG and RXRA (Agpat2-En1-motif, Dgat2-En4-motif, and Pnpla2-En5-motif) was assessed after PPARG or RXRA overexpression. Data are presented as the mean $\pm$ SD from three independent experiments, and p-values were calculated using the Wilcoxon Ranksum test (*$p < .05$, **$p < .01$).

ChREBP, mediates glucose-induced *Dgat2* expression.[103] SCD1 inhibits methylation of the *Lipe* promoter, reducing *Lipe* gene expression and participating in cardiac lipolysis regulation.[104] In addition, TFs regulate gene expression by binding to specific sequences on regulatory elements.[105] SF-1 mediates ACTH, increasing the transcriptional activity of the *Lipe* gene.[106] HIF-1 directly regulates AGPAT2 expression, affecting lipid droplet synthesis and promoting cancer cell survival under hypoxic conditions and gemcitabine resistance.[107] During adipocyte differentiation, *Agpat2* gene expression is induced, essential for TAG accumulation. Knockdown of AGPAT2 prevents proper induction of C/EBPβ and PPARγ, crucial for adipocyte differentiation.[10] miRNAs regulate protein-coding genes by binding to mRNA 3′ untranslated regions,[108–111] leading to target mRNA degradation. lncRNA 21686 and miR-146b mimic transfection in chicken liver cells inhibits lncRNA 21686, increasing miR-146b expression, decreasing AGPAT2, and regulating lipid metabolism.[112] miR-370 may play a pathogenic role in hepatic triglyceride accumulation by regulating SREBP-1c, DGAT2, and Cpt1α expression.[113]

Current research focuses on how these elements regulate key genes in triglyceride metabolism. Promoters initiate transcription near the start site, crucial for gene expression.[114–116] Enhancers are typically located at distal cis-regulatory elements, enhancing the transcription of target genes through chromatin interactions, and deletion of enhancers can partially reduce gene expression.[117] Enhancers exhibit temporal and spatial specificity, enabling them to regulate the expression of target genes in specific tissues or cell types.[118,119] In addition to super-enhancers regulating multiple genes within the same chromatin structure, most typical enhancers achieve precise control of individual target gene expression through specific chromatin loop structures. Although some enhancers associated with lipid metabolism have been identified,[57,120–122] the functional enhancers for key genes in TG metabolism—and the regulatory mechanisms governing their expression—remain largely unexplored. In the present study, we identified six functional enhancers for *Agpat2*, *Dgat2*, and *Pnpla2*, and investigated the impact of their inhibition on TG metabolism and adipocyte differentiation. This study identifies 11 active enhancers regulating key genes involved in triglyceride metabolism (*Agpat2*, *Dgat1*, *Dgat2*, *Pnpla2*, and *Lipe*) from the perspective of enhancers and investigates the regulatory functions of six enhancers with the highest activity on target gene expression. The study shows that inhibiting enhancer activity downregulates the relative expression levels of target genes, affecting adipocyte differentiation and triglyceride deposition. Our research demonstrates the ability of enhancers to regulate gene expression in lipid metabolism, providing new insights and a theoretical basis for studying lipid metabolism-related content.

The mechanism by which enhancers regulate gene transcriptional expression is currently receiving increased attention. Extensive research has demonstrated that TFs exert their influence on enhancer activity by binding to precise sites within enhancer regions, thus orchestrating gene expression.[49,123,124] In the present study, we observed that PPARG and RXRA overexpression increased the transcriptional activity of Agpat2-En1, Dgat2-En4, and Pnpla2-En5. Furthermore, compared with the control group with intact PPARG and RXRA binding sites, groups in which the shared binding sites of PPARG and RXRA within the enhancer regions were deleted showed decreased Agpat2-En1 and Dgat2-En4 activity. These findings suggest that PPARG and RXRA have crucial regulatory roles in Agpat2-En1, Dgat2-En4, and Pnpla2-En5 activity, which is similar to the results from other studies on enhancers involved in adipocyte differentiation and lipid metabolism.[125–127] Studies have indicated that, during 3T3-L1 adipogenic differentiation, PPARG and RXRA serve as the principal TFs for adipocyte differentiation and TG deposition.[74,125,128,129] Additionally, our recent research has demonstrated that PPARG and RXRA influence the activity of a *Cebpa* enhancer (Cebpa-L1-AD-En2) during adipogenic differentiation.[125] Studies have also revealed that the functionality of adipocyte-specific enhancers relies on PPARG and RXRA binding.[130,131] During adipocyte differentiation, PPARG binds to its own gene loci, including the

Pparg2 promoter and downstream intergenic enhancer regions. On Day 2 of adipogenesis, 11 280 active enhancers bind to the adipogenic TFs PPARG, CEBPA, or CEBPB, thus influencing adipogenesis.[126,132] Furthermore, Madsen et al. used the IMAGE tool in conjunction with RNA-seq, ChIP-seq of MED1, and DNase-seq data to predict that PPARG can bind to enhancers during adipocyte differentiation.[127] Together, these results imply that PPARG and RXRA can affect the activity of enhancers specific to adipocyte differentiation and lipid deposition, and are crucial TFs in adipocyte differentiation.

In summary, we identified functional enhancers for *Agpat2*, *Dgat1*, *Dgat2*, *Pnpla2*, and *Lipe* in adipocytes and investigated their roles in gene expression regulation and lipid metabolism. Furthermore, we revealed the involvement of PPARG and RXRA in the regulation of Agpat2-En1, Dgat2-En4, and Pnpla2-En5 activity. These findings deepen our understanding of the role of enhancers in TG metabolism in adipocytes, provide a theoretical basis for further explorations into the molecular mechanisms of fat deposition, and offer new perspectives for the treatment of lipid-related metabolic disorders such as hyperlipidemia, insulin resistance, fatty liver, and glucose metabolism disorders.

AUTHOR CONTRIBUTIONS

Experimental design: Keren Long and Mingzhou Li; experiment execution: Sha Zeng, Ziqi Li, and Xiaokai Li; bioinformatics: Sha Zeng, Qinjiao Du, Songling Zhang, and Haoming Wang; data analysis: Sha Zeng, Yu Zhang, and Zhining Zhong; manuscript preparation: Sha Zeng, Ziqi Li, and Xiaokai Li; review and editing: Keren Long, Mingzhou Li, Penghao Li, Anan Jiang, Peng Shang, Haohuan Li, and Xiaokai Li. All author read and approved the final version of the manuscript to be published.

ACKNOWLEDGMENTS

FUNDING INFORMATION

DISCLOSURES

The authors declare no conflicts of interest.

DATA AVAILABILITY STATEMENT

The publicly available data used in this research were obtained from the Gene Expression Omnibus (GEO) at https://www.ncbi.nlm.nih.gov/geo/. Detailed information about the public datasets used in this study is provided in Table S2. All RNA-seq data generated in this study have been submitted to the GEO database and can be accessed through the accession number GSE259270.

ETHICS APPROVAL AND CONSENT TO PARTICIPATE

Not applicable.

CONSENT FOR PUBLICATION

Not applicable.

ORCID

Sha Zeng https://orcid.org/0009-0007-5232-1753
Ziqi Li https://orcid.org/0009-0001-1476-6467
Xiaokai Li https://orcid.org/0009-0000-9380-7345
Qinjiao Du https://orcid.org/0009-0006-6601-9953
Yu Zhang https://orcid.org/0000-0001-6761-518X
Zhining Zhong https://orcid.org/0009-0001-6732-7142
Haoming Wang https://orcid.org/0009-0006-9556-7991
Songling Zhang https://orcid.org/0009-0001-3410-4284
Penghao Li https://orcid.org/0000-0003-2866-539X
Haohuan Li https://orcid.org/0009-0000-1771-3486
Li Chen https://orcid.org/0009-0004-8611-7230
Anan Jiang https://orcid.org/0000-0002-5103-4361
Peng Shang https://orcid.org/0000-0001-5427-7986
Mingzhou Li https://orcid.org/0000-0001-8681-7684
Keren Long https://orcid.org/0009-0008-0679-3095

REFERENCES

1. Mathew H, Castracane VD, Mantzoros C. Adipose tissue and reproductive health. *Metabolism*. 2018;86:18-32.
2. Fantuzzi G. Adipose tissue, adipokines, and inflammation. *J Allergy Clin Immunol*. 2005;115:911-919.
3. Pond CM. Adipose tissue and the immune system. *Prostaglandins Leukot Essent Fatty Acids*. 2005;73:17-30.
4. Luo L, Liu M. Adipose tissue in control of metabolism. *J Endocrinol*. 2016;231:R77-R99.
5. Alves-Bezerra M, Cohen DE. Triglyceride metabolism in the liver. *Compr Physiol*. 2017;8:1.
6. Demignot S, Beilstein F, Morel E. Triglyceride-rich lipoproteins and cytosolic lipid droplets in enterocytes: key players in intestinal physiology and metabolic disorders. *Biochimie*. 2014;96:48-55.

7. Nye C, Kim J, Kalhan SC, Hanson RW. Reassessing triglyceride synthesis in adipose tissue. *Trends Endocrinol Metab*. 2008;19:356-361.

8. Agarwal AK, Arioglu E, De Almeida S, et al. AGPAT2 is mutated in congenital generalized lipodystrophy linked to chromosome 9q34. *Nat Genet*. 2002;31:21-23.

9. Vogel P, Read R, Hansen G, et al. Pathology of congenital generalized lipodystrophy in *Agpat2$^{-/-}$* mice. *Vet Pathol*. 2011;48:642-654.

10. Gale SE, Frolov A, Han X, et al. A regulatory role for 1-acylglycerol-3-phosphate-O-acyltransferase 2 in adipocyte differentiation. *J Biol Chem*. 2006;281:11082-11089.

11. Sharma AK, Wolfrum C. DGAT inhibition at the post-absorptive phase reduces plasma FA by increasing FA oxidation. *EMBO Mol Med*. 2023;e18209.

12. Guo P, Yao X, Jin X, et al. Interference with DGAT gene inhibited TAG accumulation and lipid droplet synthesis in bovine Preadipocytes. *Animals*. 2023;13:2223.

13. Chitraju C, Walther TC, Farese RV. The triglyceride synthesis enzymes DGAT1 and DGAT2 have distinct and overlapping functions in adipocytes. *J Lipid Res*. 2019;60:1112-1120.

14. Sharma AK, Wang T, Othman A, et al. Basal re-esterification finetunes mitochondrial fatty acid utilization. *Molecular Metabolism*. 2023;71:101701.

15. Brügger B, Erben G, Sandhoff R, Wieland FT, Lehmann WD. Quantitative analysis of biological membrane lipids at the low picomole level by nano-electrospray ionization tandem mass spectrometry. *Proc Natl Acad Sci*. 1997;94:2339-2344.

16. Yu YH, Ginsberg HN. The role of acyl-CoA:diacylglycerol acyltransferase (DGAT) in energy metabolism. *Ann Med*. 2004;36:252-261.

17. Kelpe CL, Johnson LM, Poitout V. Increasing triglyceride synthesis inhibits glucose-induced insulin secretion in isolated rat islets of Langerhans: a study using adenoviral expression of Diacylglycerol acyltransferase. *Endocrinology*. 2002;143:3326-3332.

18. Suzuki R, Tobe K, Aoyama M, et al. Expression of DGAT2 in white adipose tissue is regulated by central leptin action. *J Biol Chem*. 2005;280:3331-3337.

19. Denison H, Nilsson C, Kujacic M, et al. Proof of mechanism for the DGAT1 inhibitor AZD7687: results from a first-time-in-human single-dose study. *Diabetes Obes Metab*. 2013;15:136-143.

20. Chitraju C, Mejhert N, Haas JT, et al. Triglyceride synthesis by DGAT1 protects adipocytes from lipid-induced ER stress during lipolysis. *Cell Metab*. 2017;26:407-418.e403.

21. Haemmerle G, Lass A, Zimmermann R, et al. Defective lipolysis and altered energy metabolism in mice lacking adipose triglyceride lipase. *Science*. 2006;312:734-737.

22. Ahmadian M, Duncan RE, Varady KA, et al. Adipose overexpression of desnutrin promotes fatty acid use and attenuates diet-induced obesity. *Diabetes*. 2009;58:855-866.

23. Holm C, Kirchgessner TG, Svenson KL, et al. Hormone-sensitive lipase: sequence, expression, and chromosomal localization to 19 cent-q13. 3. *Science*. 1988;241:1503-1506.

24. Kolditz C-I, Langin D. Adipose tissue lipolysis. *Curr Opin Clin Nutr Metab Care*. 2010;13:377-381.

25. Arner P, Langin D. The role of neutral lipases in human adipose tissue lipolysis. *Curr Opin Lipidol*. 2007;18:246-250.

26. Ambele MA, Dessels C, Durandt C, Pepper MS. Genome-wide analysis of gene expression during adipogenesis in human adipose-derived stromal cells reveals novel patterns of gene expression during adipocyte differentiation. *Stem Cell Res*. 2016;16:725-734.

27. Zimmermann R, Strauss JG, Haemmerle G, et al. Fat mobilization in adipose tissue is promoted by adipose triglyceride lipase. *Science*. 2004;306:1383-1386.

28. Kaneko K, Kuroda H, Izumi R, et al. A novel mutation in PNPLA2 causes neutral lipid storage disease with myopathy and triglyceride deposit cardiomyovasculopathy: a case report and literature review. *Neuromuscul Disord*. 2014;24:634-641.

29. Schreiber R, Xie H, Schweiger M. Of mice and men: the physiological role of adipose triglyceride lipase (ATGL). *Biochim Biophys Acta Mol Cell Biol Lipids*. 2019;1864:880-899.

30. Kraemer FB, Shen W-J. Hormone-sensitive lipase knockouts. *Nutr Metab*. 2006;3:1-7.

31. Brejchova K, Radner FPW, Balas L, et al. Distinct roles of adipose triglyceride lipase and hormone-sensitive lipase in the catabolism of triacylglycerol estolides. *Proc Natl Acad Sci*. 2021;118:e2020999118.

32. Haemmerle G, Zimmermann R, Hayn M, et al. Hormone-sensitive lipase deficiency in mice causes diglyceride accumulation in adipose tissue, muscle, and testis. *J Biol Chem*. 2002;277:4806-4815.

33. Mulder H, Sorhede-Winzell M, Contreras JA, et al. Hormone-sensitive lipase null mice exhibit signs of impaired insulin sensitivity whereas insulin secretion is intact. *J Biol Chem*. 2003;278:36380-36388.

34. Harada K, Shen W-J, Patel S, et al. Resistance to high-fat diet-induced obesity and altered expression of adipose-specific genes in HSL-deficient mice. *Am J Physiol Endocrinol Metab*. 2003;285:E1182-E1195.

35. Osuga J-I, Ishibashi S, Oka T, et al. Targeted disruption of hormone-sensitive lipase results in male sterility and adipocyte hypertrophy, but not in obesity. *Proc Natl Acad Sci*. 2000;97:787-792.

36. Panigrahi A, O'Malley BW. Mechanisms of enhancer action: the known and the unknown. *Genome Biol*. 2021;22:1-30.

37. Plank JL, Dean A. Enhancer function: mechanistic and genome-wide insights come together. *Mol Cell*. 2014;55:5-14.

38. Local A, Huang H, Albuquerque CP, et al. Identification of H3K4me1-associated proteins at mammalian enhancers. *Nat Genet*. 2018;50:73-82.

39. Calo E, Wysocka J. Modification of enhancer chromatin: what, how, and why? *Mol Cell*. 2013;49:825-837.

40. Tafessu A, Banaszynski LA. Establishment and function of chromatin modification at enhancers. *Open Biol*. 2020;10:200255.

41. Creyghton MP, Cheng AW, Welstead GG, et al. Histone H3K27ac separates active from poised enhancers and predicts developmental state. *Proc Natl Acad Sci*. 2010;107:21931-21936.

42. Kang Y, Kim YW, Kang J, Kim A. Histone H3K4me1 and H3K27ac play roles in nucleosome eviction and eRNA transcription, respectively, at enhancers. *FASEB J*. 2021;35:e21781.

43. ENCODE Project Consortium. An integrated encyclopedia of DNA elements in the human genome. *Nature*. 2012;489:57-74.

44. Beacon TH, Delcuve GVP, López C, et al. The dynamic broad epigenetic (H3K4me3, H3K27ac) domain as a mark of essential genes. *Clin Epigenetics*. 2021;13:1-17.

45. Smith E, Shilatifard A. Enhancer biology and enhanceropathies. *Nat Struct Mol Biol*. 2014;21:210-219.

46. Song L, Crawford GE. DNase-seq: a high-resolution technique for mapping active gene regulatory elements across the genome from mammalian cells. *Cold Spring Harb Protoc*. 2010;2010:pdb. prot5384.

47. Qu K, Zaba LC, Giresi PG, et al. Individuality and variation of personal regulomes in primary human T cells. *Cell Systems*. 2015;1:51-61.

48. Buenrostro JD, Wu B, Chang HY, Greenleaf WJ. ATAC-seq: a method for assaying chromatin accessibility genome-wide. *Curr Protoc Mol Biol*. 2015;109:21.29.21-21.29.29.

49. Spitz F, Furlong EE. Transcription factors: from enhancer binding to developmental control. *Nat Rev Genet*. 2012;13:613-626.

50. Rao S, Ahmad K, Ramachandran S. Cooperative binding between distant transcription factors is a hallmark of active enhancers. *Mol Cell*. 2021;81:1651-1665.e4.

51. Meng H, Bartholomew B. Emerging roles of transcriptional enhancers in chromatin looping and promoter-proximal pausing of RNA polymerase II. *J Biol Chem*. 2018;293:13786-13794.

52. Raisner R, Kharbanda S, Jin L, et al. Enhancer activity requires CBP/P300 bromodomain-dependent histone H3K27 acetylation. *Cell Rep*. 2018;24:1722-1729.

53. Richter WF, Nayak S, Iwasa J, Taatjes DJ. The mediator complex as a master regulator of transcription by RNA polymerase II. *Nat Rev Mol Cell Biol*. 2022;23:732-749.

54. Lewis MA-O, Li SA-O, Franco HA-O. Transcriptional control by enhancers and enhancer RNAs. *Transcription*. 2019;10:171-186.

55. Kim TK, Hemberg M, Gray JM. Enhancer RNAs: a class of long noncoding RNAs synthesized at enhancers. *Cold Spring Harb Perspect Biol*. 2015;7:a018622.

56. LeBlanc SE, Wu Q, Lamba P, Sif S, Imbalzano AN. Promoter–enhancer looping at the PPARγ2 locus during adipogenic differentiation requires the Prmt5 methyltransferase. *Nucleic Acids Res*. 2016;44:5133-5147.

57. Siersbæk R, Madsen JGS, Javierre BM, et al. Dynamic rewiring of promoter-anchored chromatin loops during adipocyte differentiation. *Mol Cell*. 2017;66:420-435.e5.

58. Armour SM, Remsberg JR, Damle M, et al. An HDAC3-PROX1 corepressor module acts on HNF4α to control hepatic triglycerides. *Nat Commun*. 2017;8:549.

59. Zhang L, Zhao S, Liu Y, Lv F, Geng X. Identification and validation of transcription factor-driven enhancers of genes related to lipid metabolism in metastatic oral squamous cell carcinomas. *BMC Oral Health*. 2022;22:126.

60. Green H, Meuth M. An established pre-adipose cell line and its differentiation in culture. *Cell*. 1974;3:127-133.

61. Sadowski HB, Wheeler T, Young D. Gene expression during 3T3-L1 adipocyte differentiation. Characterization of initial responses to the inducing agents and changes during commitment to differentiation. *J Biol Chem*. 1992;267:4722-4731.

62. Zhang Y, Wong C-H, Birnbaum RY, et al. Chromatin connectivity maps reveal dynamic promoter–enhancer long-range associations. *Nature*. 2013;504:306-310.

63. Schoenfelder S, Fraser P. Long-range enhancer–promoter contacts in gene expression control. *Nat Rev Genet*. 2019;20:437-455.

64. Haeussler M, Schönig K, Eckert H, et al. Evaluation of off-target and on-target scoring algorithms and integration into the guide RNA selection tool CRISPOR. *Genome Biol*. 2016;17:148.

65. Liu H, Wei Z, Dominguez A, Li Y, Wang X, Qi LS. CRISPR-ERA: a comprehensive design tool for CRISPR-mediated gene editing, repression and activation. *Bioinformatics (Oxford, England)*. 2015;31:3676-3678.

66. Labun K, Montague TG, Krause M, Torres Cleuren YN, Tjeldnes H, Valen E. CHOPCHOP v3: expanding the CRISPR web toolbox beyond genome editing. *Nucleic Acids Res*. 2019;47:W171-W174.

67. Hodgkins A, Farne A, Perera S, et al. WGE: a CRISPR database for genome engineering. *Bioinformatics (Oxford, England)*. 2015;31:3078-3080.

68. Bae S, Park J, Kim J-S. Cas-OFFinder: a fast and versatile algorithm that searches for potential off-target sites of Cas9 RNA-guided endonucleases. *Bioinformatics (Oxford, England)*. 2014;30:1473-1475.

69. Hu H, Miao Y-R, Jia L-H, Yu Q-Y, Zhang Q, Guo A-Y. AnimalTFDB 3.0: a comprehensive resource for annotation and prediction of animal transcription factors. *Nucleic Acids Res*. 2019;47:D33-D38.

70. Fornes O, Castro-Mondragon JA, Khan A, et al. JASPAR 2020: update of the open-access database of transcription factor binding profiles. *Nucleic Acids Res*. 2020;48:D87-d92.

71. Hirata T, Unoki H, Bujo H, Ueno K, Saito Y. Activation of diacylglycerol O-acyltransferase 1 gene results in increased tumor necrosis factor-α gene expression in 3T3-L1 adipocytes. *FEBS Lett*. 2006;580:5117-5121.

72. Pei Y, Song Y, Wang B, et al. Integrated lipidomics and RNA sequencing analysis reveal novel changes during 3T3-L1 cell adipogenesis. *PeerJ*. 2022;10:e13417.

73. Lee J-E, Park Y-K, Park S, et al. Brd4 binds to active enhancers to control cell identity gene induction in adipogenesis and myogenesis. *Nat Commun*. 2017;8:2217.

74. Brown JD, Feldman ZB, Doherty SP, et al. BET bromodomain proteins regulate enhancer function during adipogenesis. *Proc Natl Acad Sci*. 2018;115:2144-2149.

75. Kagey MH, Newman JJ, Bilodeau S, et al. Mediator and cohesin connect gene expression and chromatin architecture. *Nature*. 2010;467:430-435.

76. Ramasamy S, Aljahani A, Karpinska MA, et al. The mediator complex regulates enhancer-promoter interactions. *Nat Struct Mol Biol*. 2023;30:991-1000.

77. Dixon JR, Selvaraj S, Yue F, et al. Topological domains in mammalian genomes identified by analysis of chromatin interactions. *Nature*. 2012;485:376-380.

78. Jin F, Li Y, Dixon JR, et al. A high-resolution map of the three-dimensional chromatin interactome in human cells. *Nature*. 2013;503:290-294.

79. Dekker J, Marti-Renom MA, Mirny LA. Exploring the three-dimensional organization of genomes: interpreting chromatin interaction data. *Nat Rev Genet*. 2013;14:390-403.

80. Zheng H, Xie W. The role of 3D genome organization in development and cell differentiation. *Nat Rev Mol Cell Biol*. 2019;20:535-550.

81. Schmitt AD, Hu M, Jung I, et al. A compendium of chromatin contact maps reveals spatially active regions in the human genome. *Cell Rep*. 2016;17:2042-2059.

82. Fraser J, Ferrai C, Chiariello AM, et al. Hierarchical folding and reorganization of chromosomes are linked to transcriptional changes in cellular differentiation. *Mol Syst Biol*. 2015;11:852.

83. Dixon JR, Jung I, Selvaraj S, et al. Chromatin architecture reorganization during stem cell differentiation. *Nature*. 2015;518:331-336.

84. Chen L, Fish AE, Capra JA. Prediction of gene regulatory enhancers across species reveals evolutionarily conserved sequence properties. *PLoS Comput Biol*. 2018;14:e1006484.

85. Visel A, Bristow J, Pennacchio LA. Enhancer identification through comparative genomics. *Semin Cell Dev Biol*. 2007;18:140-152.

86. Gasperini M, Tome JM, Shendure J. Towards a comprehensive catalogue of validated and target-linked human enhancers. *Nat Rev Genet*. 2020;21:292-310.

87. Welter D, MacArthur J, Morales J, et al. The NHGRI GWAS catalog, a curated resource of SNP-trait associations. *Nucleic Acids Res*. 2014;42:D1001-D1006.

88. Schaub MA, Boyle AP, Kundaje A, Batzoglou S, Snyder M. Linking disease associations with regulatory information in the human genome. *Genome Res*. 2012;22:1748-1759.

89. Ying P, Chen C, Lu Z, et al. Genome-wide enhancer-gene regulatory maps link causal variants to target genes underlying human cancer risk. *Nat Commun*. 2023;14:5958.

90. Gilbert LA, Horlbeck MA, Adamson B, et al. Genome-scale CRISPR-mediated control of gene repression and activation. *Cell*. 2014;159:647-661.

91. Li K, Liu Y, Cao H, et al. Interrogation of enhancer function by enhancer-targeting CRISPR epigenetic editing. *Nat Commun*. 2020;11:485.

92. Stampfel G, Kazmar T, Frank O, Wienerroither S, Reiter F, Stark A. Transcriptional regulators form diverse groups with context-dependent regulatory functions. *Nature*. 2015;528:147-151.

93. Hu E, Tontonoz P, Spiegelman BM. Transdifferentiation of myoblasts by the adipogenic transcription factors PPAR gamma and C/EBP alpha. *Proc Natl Acad Sci*. 1995;92:9856-9860.

94. Rosen ED, Sarraf P, Troy AE, et al. PPARγ is required for the differentiation of adipose tissue in vivo and in vitro. *Mol Cell*. 1999;4:611-617.

95. Tontonoz P, Graves RA, Budavari AI, et al. Adipocyte-specific transcription factor ARF6 is a heterodimeric complex of two nuclear hormone receptors, PPAR7 and RXRa. *Nucleic Acids Res*. 1994;22:5628-5634.

96. Duncan RE, Ahmadian M, Jaworski K, Sarkadi-Nagy E, Sul HS. Regulation of lipolysis in adipocytes. *Annu Rev Nutr*. 2007;27:79-101.

97. Richard AJ, White U, Elks CM, Stephens JM. Adipose tissue: physiology to metabolic dysfunction. In: Feingold KR, Anawalt B, Blackman MR, et al., eds. *Endotext*. MDText.com, Inc; 2020.

98. Cooper G, Adams K. *The Cell: a Molecular Approach*. Oxford University Press; 2022.

99. Wray GA, Hahn MW, Abouheif E, et al. The evolution of transcriptional regulation in eukaryotes. *Mol Biol Evol*. 2003;20:1377-1419.

100. Butler JE, Kadonaga JT. The RNA polymerase II core promoter: a key component in the regulation of gene expression. *Genes Dev*. 2002;16:2583-2592.

101. Lee TI, Young RA. Transcriptional regulation and its misregulation in disease. *Cell*. 2013;152:1237-1251.

102. Casamassimi A, Federico A, Rienzo M, Esposito S, Ciccodicola A. Transcriptome profiling in human diseases: new advances and perspectives. *Int J Mol Sci*. 2017;18:1652.

103. Shin E, Bae J-S, Han J-Y, et al. Hepatic DGAT2 gene expression is regulated by the synergistic action of ChREBP and SP1 in HepG2 cells. *Animal Cells and Systems*. 2016;20:7-14.

104. Olichwier A, Sowka A, Balatskyi VV, Gan A-M, Dziewulska A, Dobrzyn P. SCD1-related epigenetic modifications affect hormone-sensitive lipase (Lipe) gene expression in cardiomyocytes. *Biochim Biophys Acta Mol Cell Res*. 2024;1871:119608.

105. Hobert O. Common logic of transcription factor and microRNA action. *Trends Biochem Sci*. 2004;29:462-468.

106. Kulcenty K, Holysz M, Trzeciak W. SF-1 (NR5A1) expression is stimulated by the PKA pathway and is essential for the PKA-induced activation of LIPE expression in Y-1 cells. *Mol Cell Biochem*. 2015;408:139-145.

107. Triantafyllou E-A, Georgatsou E, Mylonis I, Simos G, Paraskeva E. Expression of AGPAT2, an enzyme involved in the glycerophospholipid/triacylglycerol biosynthesis pathway, is directly regulated by HIF-1 and promotes survival and etoposide resistance of cancer cells under hypoxia. *Biochim Biophys Acta Mol Cell Biol Lipids*. 2018;1863:1142-1152.

108. Mihailescu R. Gene expression regulation: lessons from noncoding RNAs. *RNA*. 2015;21:695-696.

109. Mendell JT. MicroRNAs: critical regulators of development, cellular physiology and malignancy. *Cell Cycle*. 2005;4:1179-1184.

110. Das SK, Stadelmeyer E, Schauer S, et al. Micro RNA-124a regulates lipolysis via adipose triglyceride lipase and comparative gene identification 58. *Int J Mol Sci*. 2015;16:8555-8568.

111. Pan S, Cui Y, Fu Z, Zhang L, Xing H. MicroRNA-128 is involved in dexamethasone-induced lipid accumulation via repressing SIRT1 expression in cultured pig preadipocytes. *J Steroid Biochem Mol Biol*. 2019;186:185-195.

112. Xing W, Li S. LncRNA ENSGALG00000021686 regulates fat metabolism in chicken hepatocytes via miR-146b/AGPAT2 pathway. *Anim Genet*. 2024;55:420-429.

113. Iliopoulos D, Drosatos K, Hiyama Y, Goldberg IJ, Zannis VI. MicroRNA-370 controls the expression of MicroRNA-122 and Cpt1α and affects lipid metabolism [S]. *J Lipid Res*. 2010;51:1513-1523.

114. Schramm L, Hernandez N. Recruitment of RNA polymerase III to its target promoters. *Genes Dev*. 2002;16:2593-2620.

115. Ilyas G, Zhao E, Liu K, et al. Macrophage autophagy limits acute toxic liver injury in mice through down regulation of interleukin-1β. *J Hepatol*. 2016;64:118-127.

116. Smith EC, Luc S, Croney DM, et al. Strict in vivo specificity of the Bcl11a erythroid enhancer. *Blood*. 2016;128:2338-2342.

117. Wittkopp PJ, Kalay G. Cis-regulatory elements: molecular mechanisms and evolutionary processes underlying divergence. *Nat Rev Genet*. 2012;13:59-69.

118. Andersson R, Sandelin A, Danko CG. A unified architecture of transcriptional regulatory elements. *Trends Genet*. 2015;31:426-433.

119. Bogdanović O, Fernandez-Miñán A, Tena JJ, et al. Dynamics of enhancer chromatin signatures mark the transition from pluripotency to cell specification during embryogenesis. *Genome Res*. 2012;22:2043-2053.

120. Oger F, Dubois-Chevalier J, Gheeraert C, et al. Peroxisome proliferator-activated receptor γ regulates genes involved in insulin/insulin-like growth factor signaling and lipid metabolism during adipogenesis through functionally distinct enhancer classes. *J Biol Chem*. 2014;289:708-722.

121. Roqueta-Rivera M, Esquejo RM, Phelan PE, et al. SETDB2 links glucocorticoid to lipid metabolism through Insig2a regulation. *Cell Metab*. 2016;24:474-484.

122. Guan D, Xiong Y, Borck PC, et al. Diet-induced circadian enhancer remodeling synchronizes opposing hepatic lipid metabolic processes. *Cell*. 2018;174:831-842.e12.

123. Zabidi MA, Stark A. Regulatory enhancer–core-promoter communication via transcription factors and cofactors. *Trends Genet*. 2016;32:801-814.

124. Liu Z, Merkurjev D, Yang F, et al. Enhancer activation requires trans-recruitment of a mega transcription factor complex. *Cell*. 2014;159:358-373.

125. Li X, Zeng S, Chen L, et al. An intronic enhancer of *Cebpa* regulates adipocyte differentiation and adipose tissue development via long-range loop formation. *Cell Prolif*. 2023;e13552.

126. Lee J-E, Wang C, Xu S, et al. H3K4 mono-and di-methyltransferase MLL4 is required for enhancer activation during cell differentiation. *Elife*. 2013;2:e01503.

127. Madsen JGS, Rauch A, Van Hauwaert EL, Schmidt SF, Winnefeld M, Mandrup S. Integrated analysis of motif activity and gene expression changes of transcription factors. *Genome Res*. 2018;28:243-255.

128. Sagara C, Takahashi K, Kagechika H, Takahashi N. Molecular mechanism of 9-cis-retinoic acid inhibition of adipogenesis in 3T3-L1 cells. *Biochem Biophys Res Commun*. 2013; 433:102-107.

129. Watanabe M, Takahashi H, Saeki Y, et al. The E3 ubiquitin ligase TRIM23 regulates adipocyte differentiation via stabilization of the adipogenic activator PPARγ. *Elife*. 2015;4:e05615.

130. Devine JH, Eubank DW, Clouthier DE, et al. Adipose expression of the phosphoenolpyruvate carboxykinase promoter requires peroxisome proliferator-activated receptor γ and 9-cis-retinoic acid receptor binding to an adipocyte-specific enhancer in vivo. *J Biol Chem*. 1999;274:13604-13612.

131. Tontonoz P, Hu E, Graves RA, Budavari AI, Spiegelman BM. mPPAR gamma 2: tissue-specific regulator of an adipocyte enhancer. *Genes Dev*. 1994;8:1224-1234.

132. Lee J-E, Ge K. Transcriptional and epigenetic regulation of PPARγ expression during adipogenesis. *Cell Biosci*. 2014;4:1-11.

SUPPORTING INFORMATION

Additional supporting information can be found online in the Supporting Information section at the end of this article.